

The Nma1 protein promotes long distance transport mediated by early endosomes in *Ustilago maydis*

Karina Schneider¹ | Theresa Farr¹ | Niko Pinter¹ | Kerstin Schmitt² | Oliver Valerius² | Gerhard H. Braus² | Jörg Kämper¹

¹Institute of Applied Biosciences, Department of Genetics, Karlsruhe Institute of Technology, Karlsruhe, Germany

²Department of Molecular Microbiology and Genetics and Göttingen Center for Molecular Biosciences (GZMB), University of Göttingen, Göttingen, Germany

Correspondence

Jörg Kämper, Institute of Applied Biosciences, Department of Genetics, Karlsruhe Institute of Technology, Fritz Haber Weg 4, 76131 Karlsruhe, Germany. Email: kaemper@kit.edu

Present address

Theresa Farr, State Academy and Research Institute for Viticulture and Fruit Cultivation, Traubenplatz 5, Weinsberg, 74189, Germany

Niko Pinter, Institute for Surgical Pathology, Medical Center-University of Freiburg, Breisacher Straße 115a, Freiburg, 79106, Germany

Abstract

Early endosomes (EEs) are part of the endocytic transport pathway and resemble the earliest class of transport vesicles between the internalization of extracellular material, their cellular distribution or vacuolar degradation. In filamentous fungi, EEs fulfill important functions in long distance transport of cargoes as mRNAs, ribosomes, and peroxisomes. Formation and maturation of early endosomes is controlled by the specific membrane-bound Rab-GTPase Rab5 and tethering complexes as CORVET (class C core vacuole/endosome tethering). In the basidiomycete *Ustilago maydis*, Rab5a is the prominent GTPase to recruit CORVET to EEs; in *rab5a* deletion strains, this function is maintained by the second EE-associated GTPase Rab5b. The tethering- and core-subunits of CORVET are essential, buttressing a central role for EE transport in *U. maydis*. The function of EEs in long distance transport is supported by the Nma1 protein that interacts with the Vps3 subunit of CORVET. The interaction stabilizes the binding of Vps3 to the CORVET core complex that is recruited to Rab5a via Vps8. Deletion of *nma1* leads to a significantly reduced number of EEs, and an increased conversion rate of EEs to late endosomes. Thus, Nma1 modulates the lifespan of EEs to ensure their availability for the various long distance transport processes.

KEYWORDS

CORVET, early endosomes, filamentous fungi, Rab-GTPases, vesicle transport

1 | INTRODUCTION

In eukaryotic cells, endosomes are key players to control the homeostasis of membrane components. They are involved in the regulation of fundamental cellular processes as nutrient uptake, membrane turnover, and development. Early endosomes (EEs) can be formed by fusion of endocytic vesicles. From EEs, cargoes may be recycled back to the plasma membrane either directly or indirectly via recycling endosomes, or mature to late endosomes as a hub for sorting to the trans-Golgi network or fusion with lysosomes or vacuolar compartments (for review, see Scott et al., 2014). In filamentous

fungi, EEs undergo long-distance bidirectional movement, and have been shown to transport diverse cargoes as mRNAs, ribosomes, and peroxisomes, and are instrumental for formation and maintenance of the filamentous cell (Abenza et al., 2009; Becht et al., 2006; Guimaraes et al., 2015; Higuchi et al., 2014; Olgeiser et al., 2019; Zander et al., 2016).

The identity of early, late, and recycling endosomes is defined by small Rab GTPases (Ras-like proteins from rat brain). Rab GTPases can switch between an inactive, GDP-bound (Rab-GDP) and an active, GTP-bound (Rab-GTP) states. The switch between the two stages is regulated by Rab-specific Guanine Nucleotide exchange

This is an open access article under the terms of the Creative Commons Attribution License, which permits use, distribution and reproduction in any medium, provided the original work is properly cited.

© 2021 The Authors. *Molecular Microbiology* published by John Wiley & Sons Ltd.

factors (GEFs) and GTPase activating proteins (GAPs). Binding of GEFs to Rab-GTPases results in dissociation of bound nucleotides and binding of the more abundant GTP nucleotides, switching the Rab-GTPase to its active state. In return, GAPs convert the Rab-GTPase to its inactive state by inducing the hydrolysis of bound GTP to GDP. The inactive Rab-GDP is kept soluble in the cytosol via its binding to the Rab Escort Protein (REP) and the Guanine Nucleotide Dissociation Inhibitor (GDI). Rab-GDP can also bind to endosomal membranes via its prenylated C-terminal domain when dissociated from its cytoplasmic chaperones; however, Rab-GDP is extracted again by means of GDI Displacement Factors (GDFs). Only interaction with their cognate GEF leads to the GTP-bound GTPase that is retained in endosomal membranes and interacts with specific sets of effector proteins that define endosomal identity and function (reviewed in Homma et al., 2021; Langemeyer et al., 2018; Pinar & Penalva, 2021).

The first Rab-GTPase has been identified in the yeast *Saccharomyces cerevisiae* (Gallwitz et al., 1983), and subsequently, Rab-GTPases have been shown to be ubiquitously present in all eukaryotes. Ever since, significant contributions to understand the function of Rab-GTPases have been made by applying fungal systems as *S. cerevisiae*, *Aspergillus nidulans*, *Neurospora crassa*, or *Ustilago maydis* (for recent review, see Pinar & Penalva, 2021).

Rab5, one of the best studied Rab-GTPases, is prominently associated with EEs. Rab5 is highly conserved from fungi to animal systems, with up to four isoforms, depending on the evolutionary stage of the organism (Christoforidis et al., 1999; Klöpffer et al., 2012; Zerial & McBride, 2001). Rab5 directs homotypic fusion events of EEs (Diaz et al., 1988) and maturation of EEs to late endosomes. The yeast *S. cerevisiae* harbors two Rab5 isoforms, Rab5a (Vps21p) and Rab5b (Ypt52p), which is typical for the basal fungi (Klöpffer et al., 2012; Pereira-Leal, 2008), and additionally Ypt53p, originating from a duplication of *VPS21* (Lazar et al., 1997). For the filamentous ascomycete *A. nidulans*, two Rab5 isoforms, RabA and RabB, have been described (Abenza et al., 2010). In *S. cerevisiae*, only the single deletion of *vps21* affects processes on a functional endocytic pathway (Singer-Krüger et al., 1994), and also for *A. nidulans*, motility of EEs is only affected in *rabB* mutants, emphasizing the prominent function of RabB in recruiting effector proteins (Abenza et al., 2010). In contrast to yeast, however, where cells deleted for all three isoforms are still viable (Singer-Krüger et al., 1994), double deletion of *rabA* and *rabB* is lethal in *A. nidulans*, arguing for an at least partially overlapping function of the two Rab5 isoforms (Abenza et al., 2010).

In the basidiomycete *U. maydis*, two Rab5-GTPases have been identified (Fuchs et al., 2006). Rab5a moves bidirectionally along microtubule tracks (Bielska, Schuster, et al., 2014) and has been frequently used as a marker protein for EEs in *U. maydis* (Baumann et al., 2012; Göhre et al., 2012; Higuchi et al., 2014; Schuster, Kilaru, Ashwin, et al., 2011; Schuster, Kilaru, Fink, et al., 2011). Deletion of *rab5a* leads to severe morphological alterations in filaments due to defects in polarized growth, and motility of EEs is abolished (Bielska, Higuchi, et al., 2014). The function of the *U. maydis* Rab5b has not been addressed yet.

During maturation of EEs to late endosomes, Rab5 is exchanged with Rab7, the determining Rab-GTPase for late endosomes. In yeast, Rab5 (Vps21p) recruits a Rab7-specific GEF (Mon1-Ccz1) to endosomal membranes to drive the nucleotide exchange in Rab7 (Ypt7p) (Langemeyer et al., 2020). The activated Rab7-GTP is then retained in the membrane. In turn, Mon1 mediates the displacement of the GEF for Rab5 (Vps21) (Poteryaev et al., 2010), which gradually leads to the transition of Rab5-positive EEs to Rab7-positive late endosomes (for recent reviews, see Homma et al., 2021; Langemeyer et al., 2018; Pinar & Penalva, 2021).

Both Rab5 and Rab7 are effectors for multi-subunit tethering complexes that are required for membrane fusion and endosome maturation, namely the CORVET complex (class C core vacuole/endosome tethering) for Rab5 on EEs and the HOPS complex (homotypic fusion and protein sorting) for Rab7 on late endosomes.

HOPS and CORVET complexes are conserved in function from unicellular eukaryotes to mammals (Perini et al., 2014), although they may interact with different GTPases or interaction partners. In *S. cerevisiae*, CORVET is an effector primarily of Vps21 (Peplowska et al., 2007), and also for *A. nidulans* it has been shown that CORVET interacts preferentially with RabB, and only to lesser extent with RabA (Abenza et al., 2010). CORVET is required for homotypic fusion and maturation of EEs, but also involved in transport processes between endosomes and vacuoles and in sorting of transported cargoes (Balderhaar et al., 2013; Peplowska et al., 2007; Perini et al., 2014; Rink et al., 2005). HOPS is required for homotypic vacuole-vacuole fusion events, or fusion of autophagosomes or Golgi-derived vesicles with the vacuole (Liang et al., 2008; Stroupe et al., 2006; Yogosawa et al., 2005, 2006).

Both tethering complexes are related and share four subunits as core components, in yeast termed Vps11p, Vps16p, Vps18p, and Vps33p. The two CORVET-specific subunits Vps3p and Vps8p bind to Rab5 proteins, while specificity of HOPS to Rab7 is mediated by the two HOPS-specific subunits Vps41p and Vps39p (reviewed in Balderhaar et al., 2013; Solinger & Spang, 2013).

The HOPS and CORVET-specific subunits are located at opposing poles related to the central positioned core subunits of the complex (Figure 1a), which allows to contact their cognate Rab-GTPases on membranes of individual endosomes as a first step for membrane fusion (Balderhaar et al., 2013; Bröcker et al., 2012; Plemel et al., 2011). Vps33p, one of the core subunits in both complexes, is a member of the Sec1/Munc18 (S/M) protein family, which promote SNARE (soluble N-ethylmaleimide-sensitive fusion protein attachment protein receptors) complex formation. SNAREs are membrane-bound protein complexes that mediate the fusion of two membranes that harbor compatible SNARE complexes. For HOPS it has been shown that it is required for assembly of SNAREs to induce membrane fusions (Torng et al., 2020; Zick & Wickner, 2016), and, based on the structural similarity, the same is postulated for CORVET.

It was proposed that, as part of endosomal maturation progress, the complexes can transform via the intermediate complexes i-HOPS (intermediate toward HOPS) with Vps8 and Vps39, and i-CORVET (intermediate toward CORVET) with Vps3 and Vps41 as "intermediate" subunits. These complexes appear only transiently in cells, but

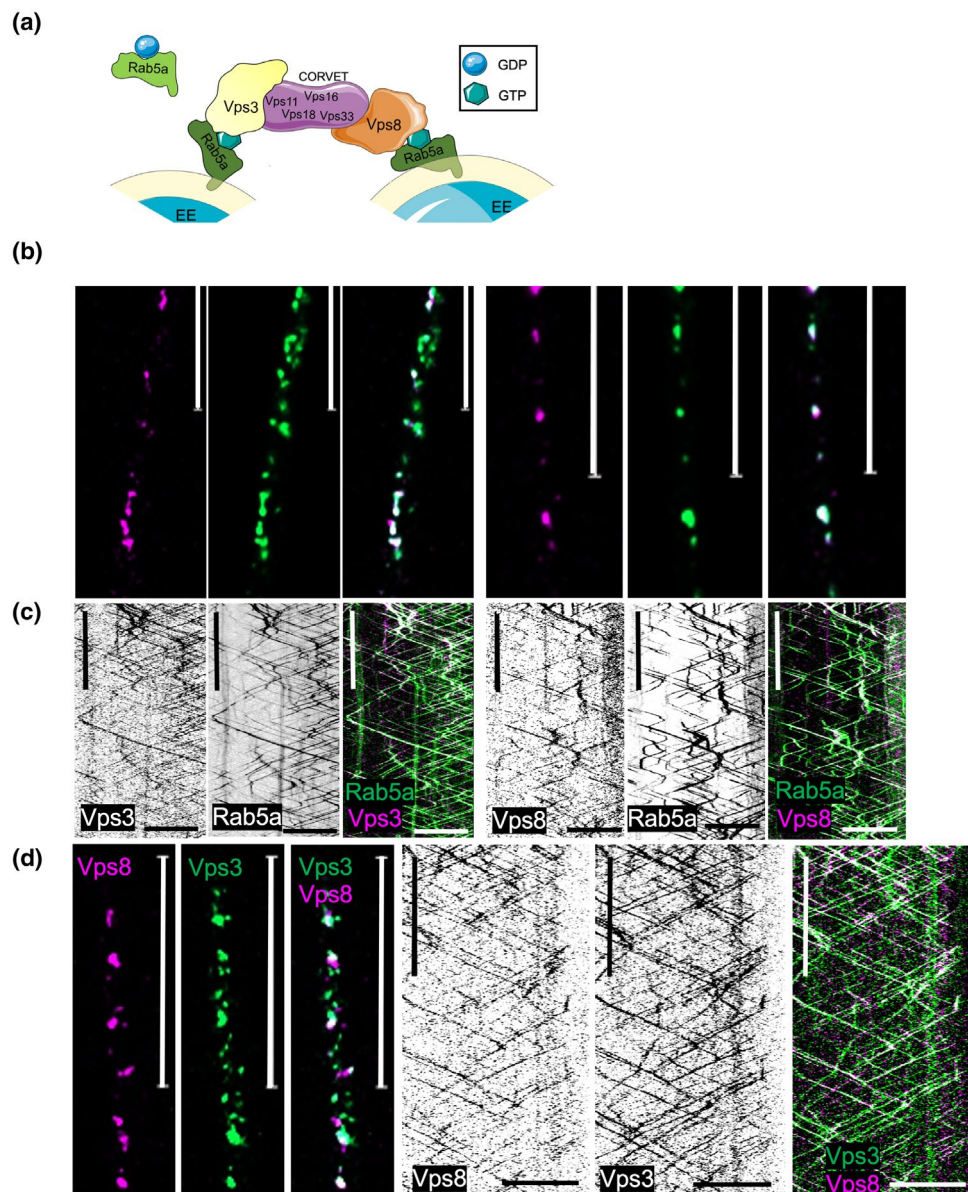


FIGURE 1 The class C core vacuole/endosome tethering (CORVET) subunits Vps3 and Vps8 colocalize in *Ustilago maydis* with early endosomes (EEs). (a) Model of the CORVET complex. CORVET binds with its specific subunits Vps3 and Vps8 to the activated form of Rab5a (GTP-bound) located on EEs to initiate endosomal fusion, indicated by arrows (Modified after Figures from Balderhaar & Ungermann, 2013). Movement of EEs is mediated by molecular motors as kinesin and dynein along the microtubule cytoskeleton. (b) Vps3 (left, mKate2, magenta) and Vps8- (right, 3xmCherry, magenta) show predominantly colocalization (white) to Rab5a (GFP, green) on EEs. (c) Kymograph showing that Vps3 (left, mKate2, magenta) and Vps8 (right, 3xmCherry, magenta) are transported with Rab5a (GFP, green) on EEs. (d) CORVET subunits Vps3 (GFP, green) and Vps8 (3xmCherry, magenta) colocalize partially (left panel, white signal) and show jointly bidirectional movement (kymograph, right panel). Kymographs: horizontal scale 10 μ m, vertical scale 10 s; Microscope pictures: Scale 10 μ m

still adopt functions in delivering cargoes to vacuoles (i-HOPS) or in recycling of material from late endosomes (i-CORVET) (Peplowska et al., 2007).

In contrast to *S. cerevisiae*, where individual components of the endocytic pathway can be deleted with only minor effects on cell growth or morphology (Singer-Krüger et al., 1994), filamentous fungi-like *A. nidulans* and *U. maydis* depend on Rab5a for polarized growth (Abenza et al., 2010; Bielska, Higuchi, et al., 2014). The elongated cells of filamentous fungi may impose additional requirements for EEs with respect to EE-mediated long distance transport within the elongated cell.

During the past decades, the basidiomycete *U. maydis* has developed to an excellent model organism for cell biological studies (summarized in Steinberg & Perez-Martin, 2008). The fungus has a dimorphic lifestyle; the switch from budding growth to filaments is controlled by the *b*-mating type locus that encodes a pair of homeodomain transcription factors, termed *bE* and *bW* (reviewed in Brefort et al., 2009). Strains in which the *bE* and *bW* genes are expressed under nutritional-controlled promoters allow the observation of both budding cells and filaments (Brachmann et al., 2001). Endosomal transport has been extensively studied in *U. maydis* and has revealed novel

functions for EEs in transport of cargoes as mRNAs, ribosomes, and peroxisomes and their impact on formation and maintenance of filamentous cells (Becht et al., 2006; Guimaraes et al., 2015; Higuchi et al., 2014; Olgeiser et al., 2019; Zander et al., 2016).

We have now studied the impact of Rab5 GTPases and the CORVET complex on function and maturation of EEs in *U. maydis*. In particular, we have identified a novel protein, Nma1, that interacts with CORVET and modulates the lifespan of EEs to ensure their availability for the various long distance transport processes.

2 | RESULTS

2.1 | The CORVET complex in *U. maydis* consists of conserved components

The components of the CORVET complex are conserved from yeasts to mammals (Perini et al., 2014), and also in *U. maydis* all components were identified in the genome based on their high similarity to both the *S. cerevisiae* and human homologs (Table S1). The composition of CORVET in *U. maydis* was investigated by co-immunoprecipitation/mass spectroscopy (Co-IP/MS). To this end, we expressed C-terminally tagged Vps3-3xHA or Vps8-3xMyc under control of the native promoter within the respective endogenous genomic locus in strain AB31. This strain allows controlled switching from budding to filamentous growth via arabinose-induced expression of the bE/bW heterodimer ($P_{\text{erg1}}:bE1$, $P_{\text{erg1}}:bW2$) (Bottin et al., 1996; Brachmann et al., 2001). When incubated under repressing conditions in glucose medium, AB31 cells multiply by budding, similar to wildtype haploid cells (sporidia). When shifted to arabinose medium, the induction of the bE1 and bW2 genes leads to the formation of the bE1/bW2 heterodimeric transcription factor that initiates filamentous growth and pathogenic development. The arabinose-induced AB31 filaments resemble the wildtype hyphae formed after fusion of compatible cells: the cells show polarized growth, but only the tip cell is filled with cytoplasm, while most of the hypha consists of empty compartments that are separated from the tip by a retraction septum (Freitag et al., 2011). In axenic culture, cells of the filaments do not divide; further development is linked to the infection of the host plant.

Proteins were extracted from either sporidia (AB31 vps3-3xHA) or filaments (AB31 vps3-3xHA and AB31 vps8-3xMyc), and Co-IP was performed with anti-HA-coupled magnetic beads or anti-Myc-coupled agarose beads. Subsequent MS analysis revealed co-purification of all CORVET components (Vps11, Vps16, Vps18, Vps33) with either Vps3-3xHA or Vps8-3xMyc, suggesting that the composition of CORVET is conserved in *U. maydis* (Table S1).

2.2 | Rab5a and the CORVET subunits Vps3 and Vps8 colocalize on EEs

To visualize the colocalization of CORVET to EEs in *U. maydis*, we constructed AB31 derivatives harboring the Rab5a protein fused

N-terminally to the green fluorescent protein (GFP), in combination with either Vps3 or Vps8 fused C-terminally to the fluorescent proteins 3xmCherry or mKate2. In all cases, the gene fusions were generated via homologous recombination at the native gene locus to ensure expression of the fusion gene under the native promoter. Movement of EEs was monitored in filamentous cells of AB31 *gfp-rab5a vps3-mKate2* and AB31 *gfp-rab5a vps8-3xmCherry*. Both Vps3-mKate2 and Vps8-3xmCherry colocalized with GFP-Rab5a on EEs (Figure 1b,c); for both proteins, only few signals were detected independent from the localization of Rab5a. In line with this, Vps8-3xmCherry and Vps3-GFP also colocalized on EEs (Figure 1d). Kymographs revealed that the colocalization of GFP-Rab5a with either Vps3-GFP or Vps8-3xmCherry occurred both during acropetal as well as basipetal movement of EEs. Our data corroborate the general scheme that the CORVET complex in *U. maydis* cells is associated with motile EEs.

2.3 | Both Rab5a and Rab5b can recruit CORVET to EEs

When compared with *S. cerevisiae* and *A. nidulans*, Rab5a from *U. maydis* is closest to Vps21p (*S.c.*) and RabA (*A.n.*), while Rab5b (*U.m.*) clusters with Ypt52 (*S.c.*) and RabB (*A.n.*) (Figures S1, S2 and Table S2). Despite the higher similarity of RabA from *A. nidulans* to Vps21p from yeast, RabB appears to be the functional ortholog of Vps21p, based on their prominent role for endosomal function (Abenza et al., 2009, 2010). Similar to Vps21, RabB, and only to a lesser extent RabA, was shown to interact with CORVET (Abenza et al., 2010; Peplowska et al., 2007). Another argument for Vps21p and RabB as orthologs is that both proteins lack a long insertion present in Ypt52 (*S.c.*) and RabA (*A.n.*). Interestingly, this extension is present in *U. maydis* Rab5a, but absent in Rab5b (Figure S1).

It has been described previously that deletion of *rab5a* in *U. maydis* abolishes movement of EEs and impedes polar growth in filaments (Bielska, Higuchi, et al., 2014). However, in contrast to these earlier observations, we still observed residual movement of EEs in AB31 filaments deleted for *rab5a*, as indicated by movement of a GFP-fusion to Yup1, a t-SNARE localizing on EEs and vacuoles (Wedlich-Söldner et al., 2000; Figure 2a,b). We also observed a cytokinesis defect in AB31 Δ *rab5a* sporidia, leading to chains of unseparated cells (Figure S3a), although growth rate of AB31 Δ *rab5a* sporidia was not altered (Figure S3c).

Despite the lack of the amino acid extension in Rab5b, which would suggest that the protein could be a functional ortholog of *A. nidulans* RabB and yeast Vps21p, the deletion of *rab5b* in AB31 did not result in detectable alterations with respect to cell morphology and growth rates (Figure S3). Furthermore, endosomal movement was not changed in AB31 Δ *rab5b*, as indicated by movement of GFP-Rab5a (AB31 Δ *rab5b gfp-rab5a*) and Yup1-GFP (AB31 Δ *rab5b yup1-gfp*; Figure S4).

We next attempted to generate strains deleted for both *rab5a* and *rab5b*. However, we never obtained transformants in efforts to delete *rab5b* in AB31 Δ *rab5a* or to delete *rab5a* in the AB31 Δ *rab5b* background, which indicates that the double deletion might be lethal.

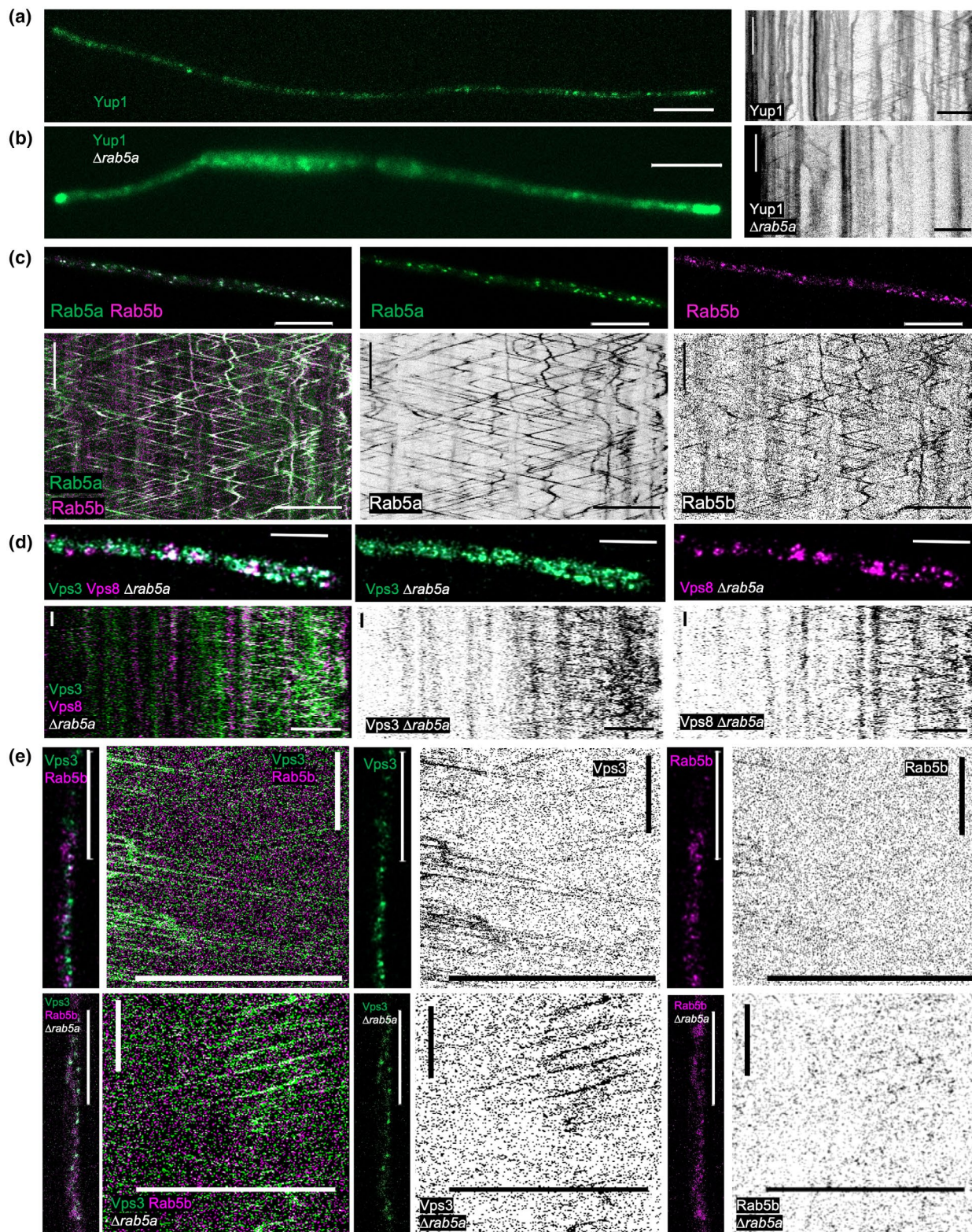
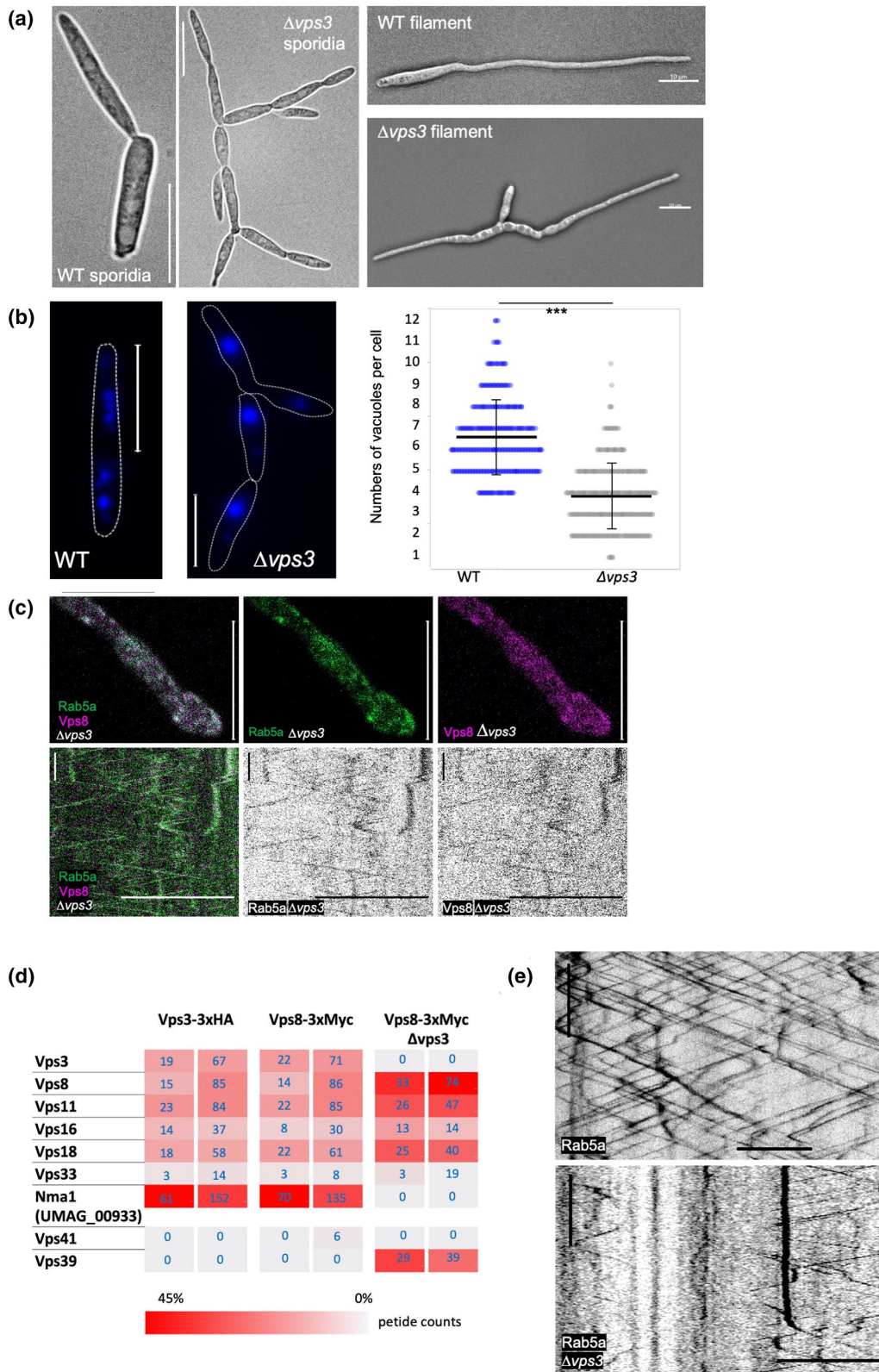


FIGURE 2 Early endosomes (EEs) show reduced, but not abolished movement in *rab5a* deletion strains. (a) In wildtype AB31 background, the t-SNARE Yup1 (GFP, green) shows evenly distribution through filaments with bidirectional movement as well as static signals. (b) Deletion of *rab5a* in AB31 results in accumulations of static Yup1 signals at cell poles of bipolar growing filaments (previously shown by Bielska, Higuchi, et al., 2014). Only in regions close to the tip of the cells bidirectional movement can be observed. (c) Rab5a (GFP, green) and Rab5b (mCherry, magenta) show colocalization (white) (upper panel) and bidirectional co-motility (lower panel). (d) Deletion of *rab5a* reduces, but does not abolish colocalization (white) (upper panel) or joint movement (lower panel) of Vps3 (GFP, green) and Vps8 (3xmCherry, magenta). (e) In wildtype AB31 hyphae (upper panel) Vps3 (GFP, green) and Rab5b (mCherry, magenta) show partial colocalization (white) and co-motility. Deletion of *rab5a* (lower panel) reduces endosomal movement, but Vps3 and Rab5b still colocalize (white) on motile EEs. Kymographs: horizontal scale 10 μ m, vertical scale 10 s



To confirm this hypothesis, we deleted *rab5a* in the haploid wildtype strain FB1 (*a1b1*) and *rab5b* in the compatible strain FB2 (*a2b2*). We inoculated maize plant seedlings with a mixture of FB1Δ*rab5a*::*nat*^R and FB2Δ*rab5b*::*gent*^R strains, and harvested diploid spores from tumor material. During germination of spores, meiosis occurs to

generate haploid sporidia. For unlinked genes, an equal distribution of the possible recombination products is expected. However, sporidia that were resistant to both Geneticin (*gent*^R) and Nourseothricin (*nat*^R) were not identified, indicative that cells with a double deletion of *rab5a* and *rab5b* are not viable (Table S3).

FIGURE 3 Deletion of *vps3* does not abolish recruitment of class C core vacuole/endosome tethering (CORVET) to early endosomes (EEs). (a) Deletion of *vps3* (right) results in cytokinesis defects in sporidia and polarity defects in AB31 Δ *vps3* hyphae, while AB31 wildtype cells (left) separate after each cell division and grow as unipolar filaments. (b) AB31 Δ *vps3* sporidia (right) contain a reduced number of vacuoles (stained with CMAC) when compared with wildtype AB31 (left). Number of vacuoles is significantly (***) reduced from 6.6 ± 1.77 in AB31 to 3.84 ± 1.55 in AB31 Δ *vps3* (arithmetic mean, standard deviation; t-test $p < .001$, $N = 300$). (c) Rab5a (GFP, green) and Vps8 (3xmCherry, magenta) show colocalization (white) (upper panel) and bidirectional co-motility (white) (lower panel) in AB31 Δ *vps3* strains. (d) Impact of a *vps3* deletion on the composition of CORVET in *Ustilago maydis*. AB31 *vps3*-3xHA, AB31 *vps8*-3xMyc, and AB31 *vps8*-3xMyc Δ *vps3* strains were analyzed by Co-IP/MS experiments in two independent biological replicates. As control, the untagged AB31 wildtype strain and either Anti-HA coupled magnetic beads or Anti-Myc coupled agarose beads were used. MS-data were analyzed with MaxQuant 1.6.0.16 (Tyanova et al., 2016) (<https://maxquant.org>). Given are peptide counts after subtraction of nonspecifically enriched peptides from control samples. Threshold for peptide counts: >5 peptides in at least one of the biological replicates. Values for AB31 *vps3*-3xHA, AB31 *vps8*-3xMyc are also given in Table S1. The color range from red (45) to grey (0) indicates the % of cumulative peptide counts. (e) Deletion of *vps3* (lower panel) in AB31 results in localization of Rab5a signals (GFP) to bidirectional motile EEs, but also result in enhanced localization at static structures when compared with wildtype AB31 (upper panel). Kymographs: horizontal scale 10 μ m, vertical scale 10 s

In addition to Rab5a and Rab5b, we have identified Rab5c as an additional protein with similarity to Rab5-GTPases. Rab5c shows 43.6% and 42.9% identity to Rab5a and Rab5b, respectively. In *S. cerevisiae*, it is most similar to Ypt53, (46.9%), a gene duplication of Vps21 (Klöpffer et al., 2012), and in *A. nidulans* to RabX, a protein with unknown function (Pinar & Penalva, 2021; Table S2). In addition to conserved domains present in the Rab5 protein family, the Rab5c protein shows an N-terminal extension of 340 amino acids and an internal insertion of 112 amino acids, both with unknown function (Figures S1 and S2).

Deletion of *rab5c* did not cause any obvious alteration of the phenotype with respect to cell morphology or movement of EEs; also, the combined deletion with *rab5a* or *rab5b* did not alter the phenotype of strains harboring single *rab5a* or *rab5b* deletions (Figure S5). The finding that in cells deleted for *rab5a* movement of EEs is severely reduced, but still observable, argues that Rab5a is the prominent Rab5-GTPase required for the function of EEs. As the double deletion of Δ *rab5a* Δ *rab5b* is lethal, the residual movement (and activity) in Δ *rab5a* strains has to be attributed to Rab5b that can partially overtake the function of Rab5a. Rab5c apparently has no influence on endosomal function or movement. In accordance with the partially redundant function of Rab5a and Rab5b, both proteins were found to colocalize on 50%–60% of the EEs in strain AB31 *gfp-rab5a mCherry-rab5b* ($N = 40$ independent hyphae; Figure 2c). For Rab5c (AB31 $P_{nar1:gfp-rab5c vps8-3xmCherry}$), no specific localization to EEs was observable (Figure S6).

We next examined the Rab5-dependent recruitment of the CORVET complex to EEs. Deletion of *rab5b* (AB31 Δ *rab5b vps3-gfp vps8-3xmCherry*) did not alter the localization of the CORVET subunits Vps3-GFP or Vps8-3xmCherry to EEs. In accordance with the central function of Rab5a, the *rab5a*-deletion in strain AB31 Δ *rab5a vps3-gfp vps8-3xmCherry* led to a severe reduction in EE motility (Figure 2d). However, Vps3 and Vps8 colocalized on the residual moving EE, emphasizing that Rab5b can complement partially the function of Rab5a in recruiting the CORVET complex to EE (Figure 2d). This is in line with the finding that Vps3 and Rab5b show colocalization on motile EEs in the *rab5a* deletion strain AB31 Δ *rab5a mCherry-rab5b vps3-gfp* (Figure 2e), demonstrating that Rab5b is sufficient to recruit CORVET to EEs in the absence of Rab5a.

2.4 | Recruitment of the CORVET complex to early endosomes is initiated by Vps8

For functional analysis of the CORVET subunits Vps3 and Vps8 and the core-subunit Vps11, we attempted to generate the respective deletion strains. As we were not able to generate haploid Δ *vps8* or Δ *vps11* strains, we deleted one copy of either *vps8* or *vps11* in the diploid, so-lopathogenic strain FBD11 (*a1a2b1b2*) (Banuett & Herskowitz, 1989). Analysis of the meiotic offspring revealed no haploid Δ *vps8* sporidia ($N = 60$) or Δ *vps11* sporidia ($N = 178$), demonstrating that both *vps8* and *vps11* are essential genes in *U. maydis* (Table S3).

Deletion of *vps3* resulted in a phenocopy of the *rab5a* deletion phenotype (Figure S3): budding cells displayed a cytokinesis defect, leading to chains of nonseparated cells (Figure 3a). Induction of filamentous growth in AB31 Δ *vps3* led to the formation of filaments on both cell poles of the sporidia (bipolar filament formation), while wildtype AB31 cells formed unipolar filaments (Figure 3a). As described for *S. cerevisiae* Δ *vps3* strains, the AB31 Δ *vps3* strains contained a reduced number of vacuolar compartments compared with wildtype cells (AB31: 6.6 ± 1.77 (standard deviation); AB31 Δ *vps3*: 3.84 ± 1.55 ; t-test $p < .001$, $N = 300$; Figure 3b).

However, deletion of *vps3* did neither abolish the movement of EEs nor recruitment of the CORVET complex to EEs: in AB31 Δ *vps3 gfp-rab5a vps8-3xmCherry*, Rab5a was localized on motile EEs and colocalized with Vps8 (Figure 3c). Apparently, similar to the situation in *S. cerevisiae*, the first step in recruitment of CORVET to EEs requires Rab5a and Vps8; Vps3 is then required for recruitment of a second Rab5a to initiate the subsequent steps in endosome maturation and/or fusion (Pawelec et al., 2010; Peplowska et al., 2007). As Vps8 is essential, we were not able to examine whether Vps3 is able to partially complement the function of Vps8 to recruit CORVET to EEs.

To examine whether deletion of *vps3* alters the composition of CORVET, we performed Co-IP/MS with protein extracts from strain AB31 Δ *vps3 vps8-3xmyc* compared with the respective wildtype strain. All components of CORVET (with exception of Vps3) co-purified with Vps8. Interestingly, when compared with the Co-IP from wildtype strains, we detected an enrichment of Vps39 in Δ *vps3* cells (Figure 3d). In yeast, during maturation of EEs to late endosomes, Vps3 is substituted by Vps39 in the CORVET-related HOPS-complex,

which is specific for late endosomes (Ostrowicz et al., 2010; Plemel et al., 2011). Our findings suggest now that deletion of *vps3* alters the specificity of CORVET by substitution of Vps3 with Vps39, which would lead to a hybrid CORVET–HOPS complex. Indeed, we observed GFP-Rab5a in $\Delta vps3$ cells increasingly associated with immobile structures that probably resemble late endosomes (Figures 3e and S7).

Interestingly, in both Vps3 and Vps8 Co-IP/MS experiments, in addition to the conserved CORVET complex components, a so far uncharacterized protein (Umag_00933) was co-purified with high abundance (Table S1 and Figure 3d).

2.5 | Nma1 (Umag_00933) interacts with CORVET and localizes at EEs and microtubules

umag_00933 encodes for an uncharacterized protein of 1290 amino acids with unknown function. Bioinformatical characterization revealed a central SMC domain (structural maintenance of chromosomes, NCBI conserved domain search, E -value $5.8 \cdot 10^{-22}$), a domain present in SMC proteins that participate in higher-order chromosome organization and dynamics (Huang et al., 2005; Losada & Hirano, 2005; Nasmyth & Haering, 2005).

BlastP analysis identified proteins similar to Umag_00933 with the highest similarities within the group of Ustilaginomycotina (best match to a SRS1_12231, a hypothetical protein from *Sporisorium reilianum*, E -value 0.0%, 65.01% identity, 100% coverage). Proteins with

less similarity (but still harboring the SMC-domain) are present in other Basidiomycota and Ascomycetes, but not outside the fungal kingdom. No proteins with significant similarities to Umag_00933 were found in budding yeasts (*Saccharomycetales*).

Based on the finding that Umag_00933 co-purified with components of CORVET, we examined the possible association of the protein with EEs in strain AB31 *umag_00933-3xmCherry gfp-rab5a*. Indeed, Umag_00933 was found to colocalize with Rab5a on motile EEs (Figure 4a). In addition, we observed a colocalization of Umag_00933 with microtubules (AB31 *umag_00933-3xgfp P_{otef}:mCherry-tub1*; Figure 4b). Also, treatment with Benomyl, a microtubule-destabilizing agent, led to disruption of the fibrillar Umag_00933 localization (Figure S8). Heterologous expression of Umag_00933-GFP in *A. nidulans* harboring a mCherry–RabA fusion protein (homologous to Rab5a) revealed that Umag_00933 also localized to fibrillar structures (microtubules). While the EE-marker RabA showed bidirectional motility, we could not detect any movement for Umag_00933, indicating that microtubule-association, but not the localization to motile EEs, is maintained in *A. nidulans* (Figure S9).

Due to the endosome- and microtubule- association of Umag_00933, we termed the protein Nma1 (N-dosome and Microtubule Associated).

In accordance with the association of Nma1 with CORVET (indicated by Co-IP, Table S1 and Figure 3d), Nma1 colocalized and moved together with both Vps3 and Vps8 (AB31 *vps3-gfp nma1-3xmCherry* and AB31 *vps8-3xmCherry nma1-3xgfp*; Figure 5a,b).

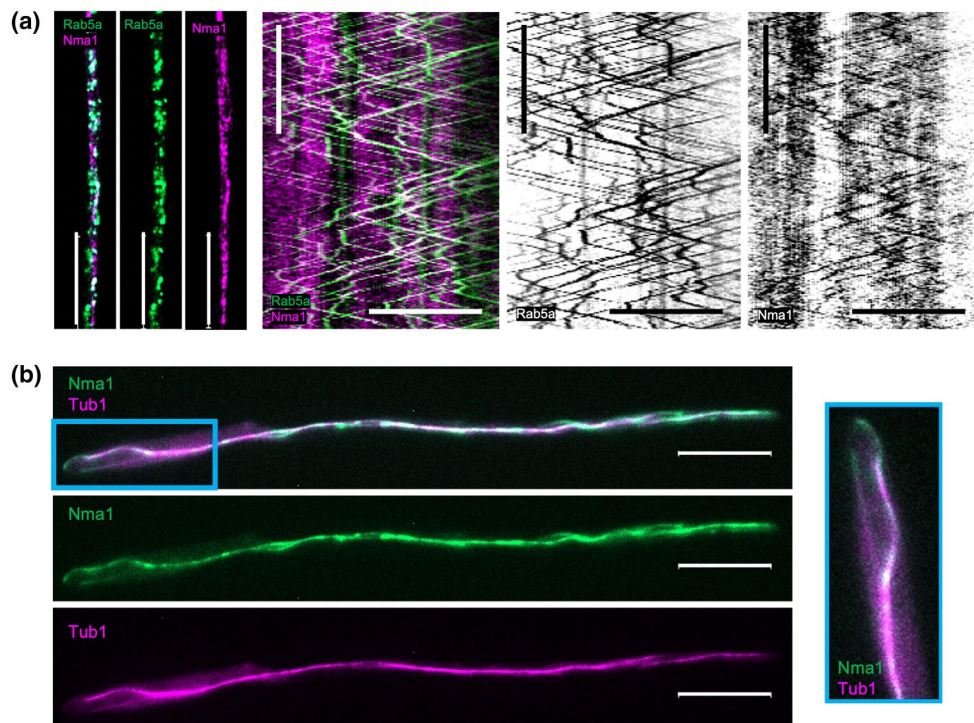


FIGURE 4 Nma1 localizes at early endosomes and microtubules. (a) Rab5a (GFP, green) and Nma1 (3xmCherry, magenta) show colocalization (white, left panel) and bidirectional co-motility (white, right panel) in AB31 strains. Nma1 localizes in addition to static structures. (b) Nma1 (GFP, green, middle panel) and Tub1 (mCherry, magenta, lower panel) show colocalization (white, upper panel) at fibrillar structures through whole AB31 hyphae. See also enlargement on the right (blue box). Kymographs: horizontal scale 10 μ m, vertical scale 10 s

Deletion of *rab5a* strongly reduced localization of both Vps3 and Nma1 to EEs and resulted in drastically diminished motility of EEs, as previously observed for $\Delta rab5a$ deletion strains (Figure 5c). While deletion of *vps3* only led to reduced motility of Rab5 or Vps8 labeled EEs (see Figure 3c), we could not detect any motility of Nma1 in *vps3* deletion strains (AB31 $\Delta vps3$ *nma1-3xgfp*; Figure 5d). Consistently, in Co-IP/MS experiments with Vps8-3xMyc, deletion of *vps3* abolished the co-purification of Nma1 together with conserved CORVET components (Figures 3d and 6a), indicating that Vps3 is required for the interaction of Nma1 with CORVET. A suggested direct interaction between Nma1 and Vps3 was further confirmed by yeast two-hybrid analysis: a 184 aa C-terminal fragment of Nma1 fused to the Gal-AD was tested in combination with either Vps3, Vps11, and Vps18 fused to Gal-DB, and only for the combination of Nma1 and Vps3 activation of the reporter genes was observed (Figure 6b).

2.6 | Deletion of *nma1* leads to a reduced number of EEs and affects the composition of CORVET

The deletion of *nma1* significantly reduced the total number of EEs from 74 ± 18 EEs ($N = 50$, visualized by GFP-Rab5a) in AB31 (WT) filaments to 48 ± 7 ($N = 48$; t -test $p < .001$) in the $\Delta nma1$ background (Figure 7a). The size of EEs was not significantly affected by the *nma1* deletion (measured by the average area of all GFP-Rab5a signals in each cell, for details see Experimental Procedures; $0.27 \pm 0.07 \mu\text{m}^2$ in WT vs. $0.28 \pm 0.069 \mu\text{m}^2$ in $\Delta nma1$, $p = .48$; Figure 7a).

Interestingly, the *nma1* deletion significantly decreased the association of Vps8 and Vps3: in wildtype AB31 hyphae $29 \pm 13\%$ of the Vps8-3xmCherry signals showed an overlap with Vps3-GFP signals (measurement of the area of respective Vps8-3xmCherry and Vps3-GFP signals in 10 independent hyphae and the distribution of separate vs. merged signals), in the respective $\Delta nma1$ hyphae the number was significantly (t -test $p < .001$) reduced to $7 \pm 7\%$ (32 independent hyphae; Figure 7b). We then analyzed the association of Rab5a with either Vps8 or Vps3: the Rab5a/Vps8 colocalization was only modestly, but not significantly reduced upon *nma1* deletion (wildtype: $54 \pm 8\%$, $N = 20$ cells; $\Delta nma1$: $46 \pm 18\%$, $N = 35$ cells, t -test $p = .0235$), whereas the colocalization of Rab5a and Vps3 was significantly decreased (wildtype: $43 \pm 13\%$, $N = 25$ cells; $\Delta nma1$: $18 \pm 21\%$, $N = 35$ cells, t -test $p < .001$; Figure 7d,e). Taken together, these results show that deletion of *nma1* reduces the association of Vps3 with the CORVET core complex on EEs.

We also observed a delocalization of Vps8 in $\Delta nma1$ hyphae: in AB31 *vps8-3xmCherry* $\Delta nma1$, Vps8 signals accumulated at the hyphal tip and the septum, and only few motile signals were observed in between (Figure 7c). The motility of Rab5a was not significantly altered in the $\Delta nma1$ strain AB31 $\Delta nma1$ *gfp-rab5a* *vps3-mKate2*. Reminiscent to the cellular distribution of Vps8, we also observed an accumulation of Rab5a at the septum and hyphal tip (Figure S10).

2.7 | Nma1 deletion leads to an increased conversion rate of EEs to late endosomes

Rab7 is the GTPase localized on late endosomes, and simultaneous localization with Rab5a is associated with the conversion process from early to late endosomes (Casanova & Winckler, 2017; Rink et al., 2005; Shearer & Petersen, 2019). In wildtype-cells, about $5 \pm 3\%$ of endosomes showed an overlapping signal of GFP-Rab5a and mCherry-Rab7 (measurement of 20 independent hyphae). In $\Delta nma1$ hyphae, the co-localization of the two proteins increased significantly to $27 \pm 7\%$ (t -test: $p < .001$, 40 independent hyphae) (Figure 8a). Thus, deletion of *nma1* leads to an increased conversion to late endosomes. The number of Rab7-marked late endosomes was found to be significantly reduced (wildtype: 121.7 ± 51 , $N = 20$ cells; $\Delta nma1$: 62.8 ± 17.4 , $N = 45$ cells, t -test $p < .001$), and the size was significantly increased (wildtype: $0.289 \pm 0.2 \mu\text{m}^2$, $\Delta nma1$: $0.65 \pm 0.29 \mu\text{m}^2$, t -test: $p < .001$; Figure 8b). Apparently, similar to the effects shown for Rab5a-marked EEs, also the population of late endosomes is affected by the *nma1* deletion.

3 | DISCUSSION

For the function and maturation of EEs, tethering and fusion of membrane compartments is an essential process. Tethering is regulated via multi protein complexes such as the CORVET complex, which interacts specifically with Rab5 GTPases (reviewed in Ungermann & Kümmel, 2019). Similar to *S. cerevisiae* and *A. nidulans* (Abenza et al., 2010; Singer-Krüger et al., 1994) one of the Rab5 proteins, Rab5a, plays a more prominent role with respect to function of EEs (Figures 2 and S3). The isoforms of the Ypt5 family of Rab-GTPases in fungi has evolved by multiple, independent duplications (Pereira-Leal, 2008). Ypt51 is present in most Ascomycota and originates likely from a duplication of either Ypt52 or Ypt54 at the base of the Ascomycota branch (Figure S1c). Ypt52 and Ypt54 result probably from an early duplication of an ancestral gene, followed by an asymmetric gene loss, as fungi carry only one of the two isoforms (Pereira-Leal, 2008). In Basidiomycota, the Ypt5 isoforms appear to result from lineage-specific duplications of Ypt54 (Figure S1b,c, Pereira-Leal, 2008). Given the fact that the Rab5 isoforms with a dominant function for EEs in *A. nidulans*, *S. cerevisiae*, and *U. maydis* all belong to different branches (Vps21p: Ypt51; RabB: Ypt54; Rab5a: Ypt54; Figure S1b,c), it appears likely that this function was already accomplished by the ancestral Ypt5 protein, and that the duplicated isoforms occupied novel/altered functions.

At least some of the functions of Rab5a (with respect to endosomal movement) can be overtaken by Rab5b (Figure 2d). The redundant function of the two Rab5 GTPases is further supported by the lethal phenotype of the double deletion in *U. maydis*, and, similarly, in *A. nidulans* (Abenza et al., 2010). In *S. cerevisiae*, the double deletion of *vps21/ypt52* (equivalent to Rab5a/Rab5b) is viable (Singer-Krüger et al., 1994), which can be explained by the nonessential role of endocytosis in yeasts. Rab5c, the third Rab5-GTPase present in the *U. maydis* genome, has obviously no function

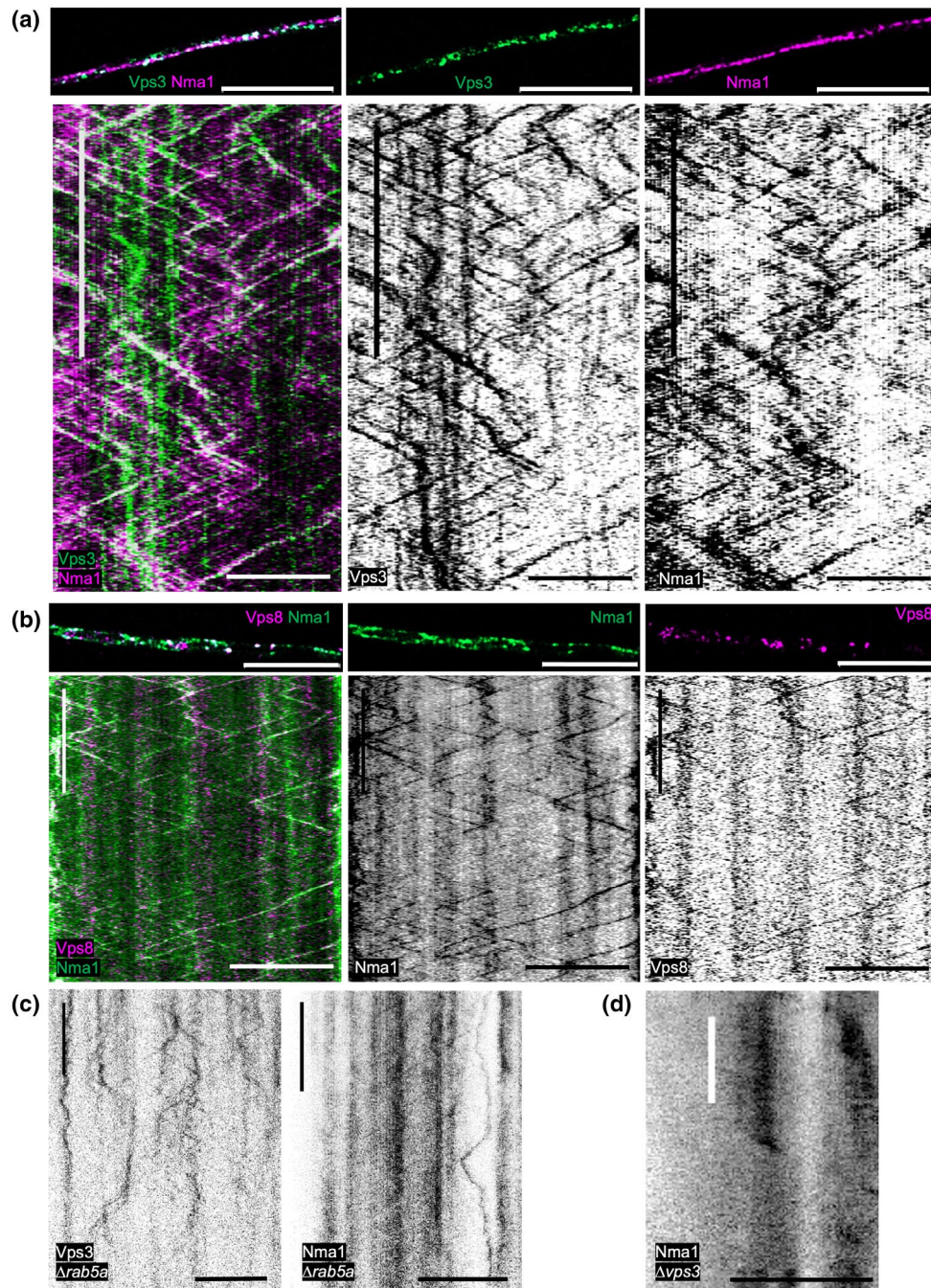


FIGURE 5 Motility of Nma1 depends on class C core vacuole/endosome tethering (CORVET) subunit Vps3. (a) CORVET subunit Vps3 (GFP, green) and Nma1 (3xmCherry, magenta) show colocalization (white) (upper panel) and bidirectional co-motility (lower panel) in AB31 strains. (b) Nma1 (GFP, green) and CORVET subunit Vps8 (3xmCherry, magenta) show colocalization (white) (upper panel) and bidirectional jointly motility (lower panel) in AB31 hyphae. (c) Deletion of *rab5a* strongly reduces, but does not inhibit bidirectional motility of Vps3 (GFP, left panel) or Nma1 (3xGFP, right panel) in AB31Δ*rab5a*. (d) Deletion of *vps3* (AB31Δ*vps3*) prevents motility of Nma1 (3xGFP). Kymographs: horizontal scale 10 μm, vertical scale 10 s

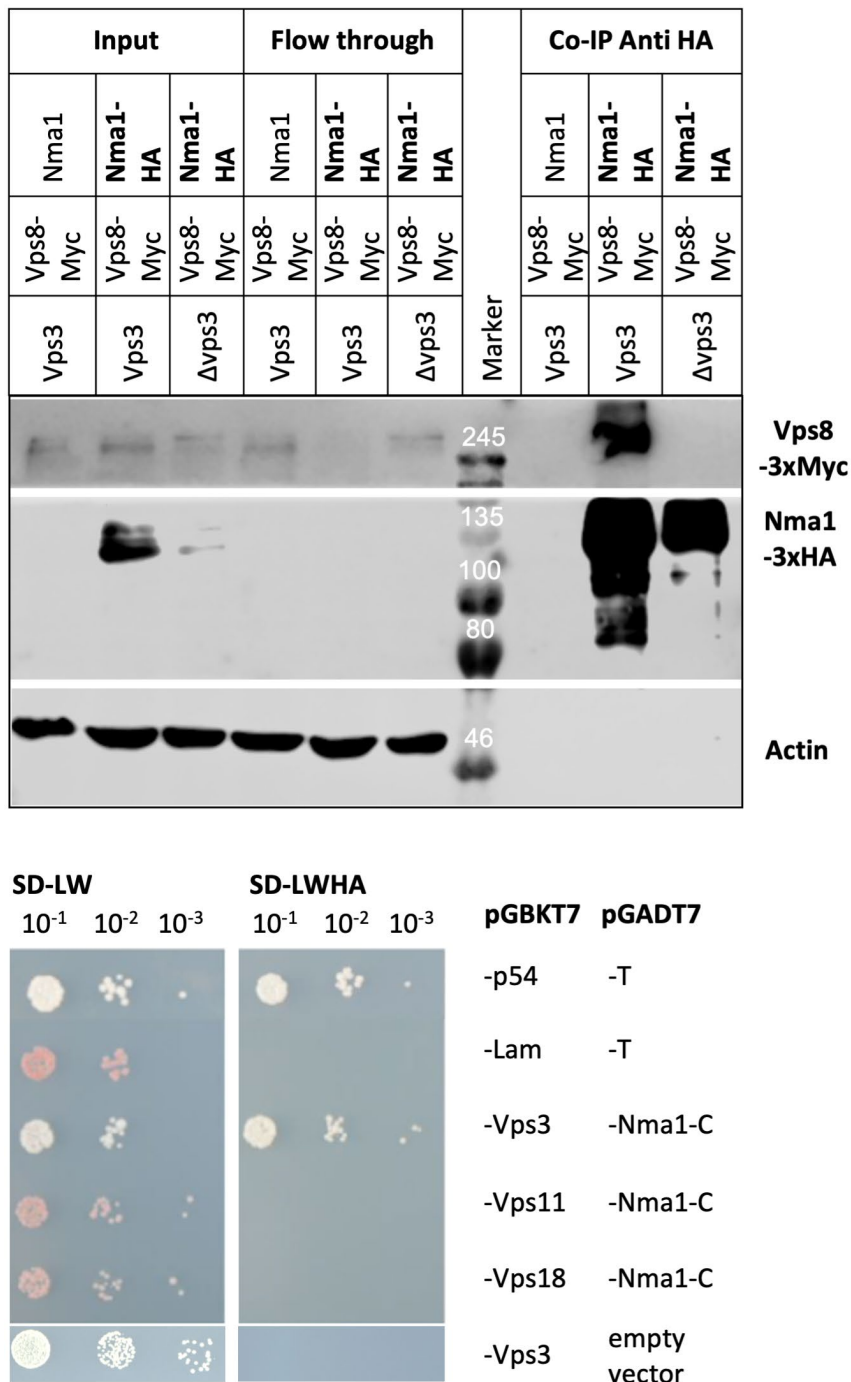
related to endosomal movement (Figure S5). The overall structure of Rab5c with the conserved Rab5 domain covering only a third of the length of the protein (Figures S1 and S2) may indicate a function independent from the other two Rab5 GTPases in *U. maydis*.

The organization of the CORVET complex in *U. maydis* with the six subunits Vps3, Vps8, Vps11, Vps16, Vps18, and Vps33 (Figure 3d) follows the general scheme described for various other organisms,

including the well-studied components from *S. cerevisiae* and mammalian cells (Peplowska et al., 2007; Perini et al., 2014). Exemptions from this conserved organization are sparse; for example, for *D. melanogaster* a “mini-CORVET” is described, which lacks the subunit Vps3 (Lörincz et al., 2016).

Identical to the known mechanisms in yeast for the assembly of the CORVET complex (Pawelec et al., 2010), the CORVET subunit

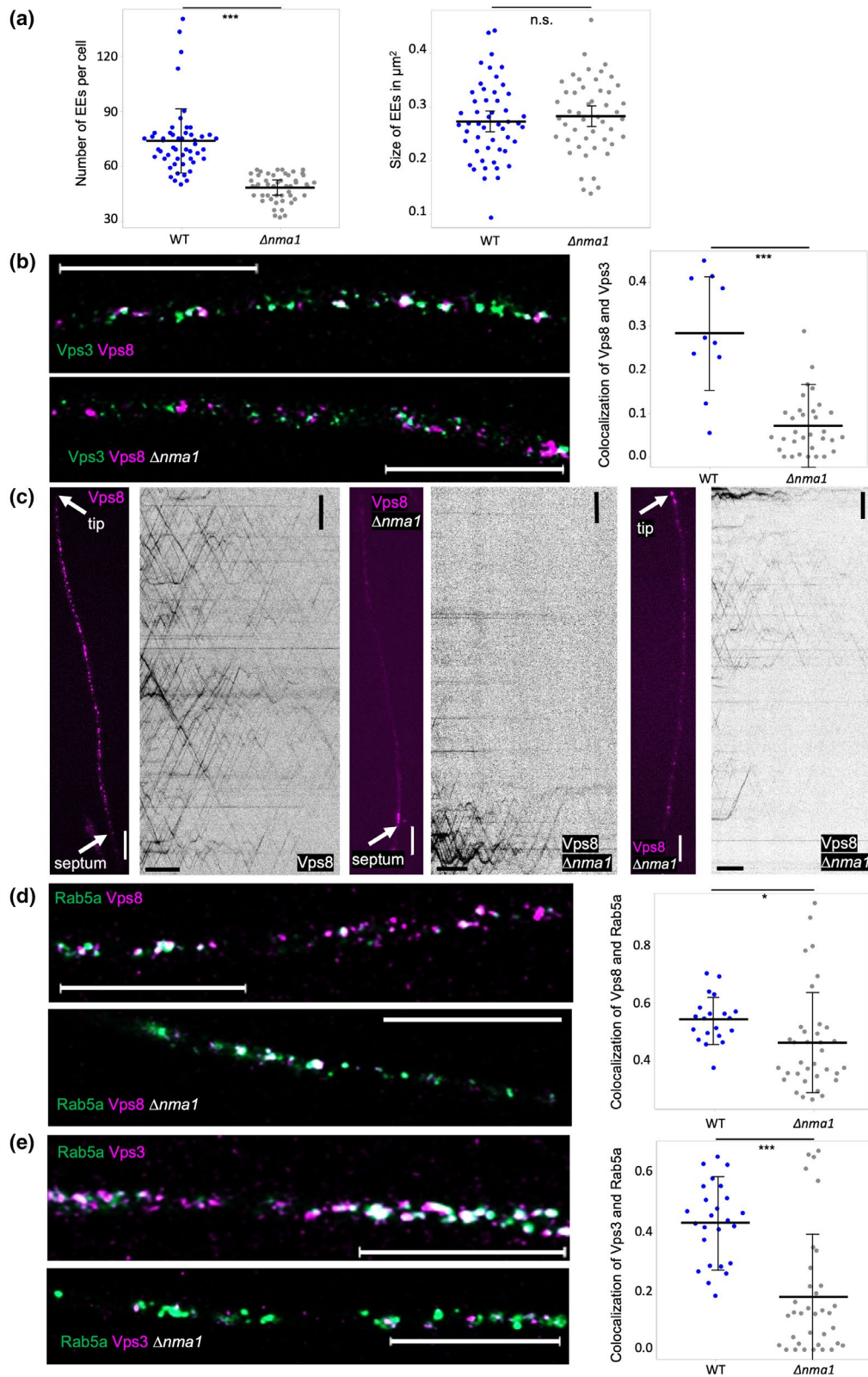
FIGURE 6 Association of Nma1 with CORVET depends on Vps3. (a) Deletion of *vps3* abolishes interaction with CORVET. Co-IP was performed with Nma1-3xHA as bait with proteins extracted from strains AB31 *nma1-3xHA vps8-3xMyc*, AB31 Δ *vps3 nma1-3xHA vps8-3xMyc*, and AB31 *vps8-3xMyc* (control with untagged bait protein). Western blot was probed with antibodies specific for Nma1-3xHA (128 kDa) Vps8-3xMyc (248 kDa) or actin (42 kDa). Vps8-3xMyc (marker protein for CORVET) co-purifies with Nma1-3xHA in wildtype background, while in the *vps3* deletion strain Vps8-3xMyc is not co-purified. (b) Nma1 interacts directly with Vps3 in the yeast two-hybrid system. Vps3, Vps11, and Vps18 were expressed from plasmid pGBKT7 (bait) in combination with a N-terminally truncated version of Nma1 (Nma1-C, corresponding to 184 amino acids of the C-terminus of Nma1) expressed from pGADT7 (prey). Transformants were spotted in tenfold dilution steps on control plates (*SD-LW*) and on plates (*SD-LWHA*) indicative for protein–protein interaction (Vps3 and Nma1-C). The combination of pGBKT7-Vps3 and the empty pGADT7 vector serves as a control for self-activation by Vps3. No interaction was detectable in strains expressing Nma1-C and Vps11 or Nma1-C and Vps18. Cells transformed with pGBKT7-p53 and pGADT7-T (interaction between p53 and T-antigen) or pGBKT7-Lam and pGADT7-T serve as positive and negative controls



Vps8 is sufficient to recruit the complex to EEs via Rab5, as evidenced by the finding that in *U. maydis* Δ *vps3*-strains Vps8 is still present on motile EEs (Figure 3c).

In contrast to *S. cerevisiae* and *A. nidulans*, where ablation of CORVET components leads to severe growth defects and an altered vacuolar morphology (Lopez-Berges et al., 2017; Marsalek et al., 2017; Pawelec et al., 2010), in *U. maydis* the ablation of Vps8, as well as ablation of the core component Vps11 is lethal. Δ *vps3* strains display a phenotype similar to Δ *rab5a* strains with severe defects in polar growth, cytokinesis, and movement of EEs (Figure 3). In yeast, the function of Vps3 is to connect the CORVET complex bound to Rab5a via Vps8 of one EE to Rab5a attached to

a second EE to initiate fusion/maturation (Balderhaar et al., 2013; Pawelec et al., 2010; Peplowska et al., 2007). Apparently, in *U. maydis* the presence of CORVET on EEs (via Vps8) appears to be more important than its function in vesicle fusion (via Vps3). This may reflect a prominent function of CORVET with respect to the long distance transport function of EEs. For both *A. nidulans* and *U. maydis*, it has been shown that the conserved fused toes (FTS)-Hook-Hook interacting protein (FHIP) complex (FHF) serves as an adapter between EEs and the dynein and kinesin motor proteins instrumental for microtubule-dependent transport of EEs. All three components of the complex are critical for movement of EEs (Bielska, Schuster, et al., 2014; Yao et al., 2014; Zhang et al., 2014).



In *A. nidulans*, it has been shown that the Hook-EE interaction is mediated by FHIP (Yao et al., 2014), and for the human FHF complex it has been described that it interacts with VPS16 and VPS18, conserved component of HOPS and CORVET (Xu et al., 2008). In mammalian cells, Rab5 has also been described to interact directly

with the FHF complex (Christensen et al., 2021; Guo et al., 2016). In fungi, it appears well feasible that CORVET is required as a connection between FHF and Rab5 to facilitate movement of EEs. The EE-mediated transport of cargoes as mRNA/polysomes, lipid droplets, peroxisomes, or the endoplasmic reticulum (Baumann

FIGURE 7 Influence of *Nma1* on the population of early endosomes (EEs). (a) In AB31 hyphae, deletion of *nma1* causes a significant reduction in the number of EE (left panel, wt: 74 ± 18 EEs, $N = 50$, visualized by GFP-Rab5a per cell; $\Delta nma1$: 48 ± 7 , $N = 48$; t -test $p < .001$) and a slightly, but not significantly, gain of EE size (right panel, wt: $0.27 \pm 0.07 \mu\text{m}^2$, $\Delta nma1$: $0.28 \pm 0.069 \mu\text{m}^2$, t -test $p = .484$). (b) Deletion of *nma1* impacts the colocalization (left panel) of class C core vacuole/endosome tethering (CORVET) subunits Vps3 (GFP, green) and Vps8 (3xmCherry, magenta). Overlap of respective fluorescence signals is decreased from $29 \pm 13\%$ in wt AB31 hyphae (measurement of 10 independent filaments) to $7 \pm 7\%$ in $\Delta nma1$ (32 independent hyphae; t -test $p < .001$). (c) CORVET subunit Vps8 (3xmCherry, magenta) shows long distance bidirectional motility (left panel) in AB31 strains. Deletion of *nma1* (AB31 $\Delta nma1$) causes accumulation of Vps8-3xmCherry signals in tip regions and at retraction septa of hyphae (middle and right panel). (d) Deletion of *nma1* marginally influences colocalization (left panel) of CORVET subunit Vps8 (3xmCherry, magenta) and Rab5a (GFP, green). Overlap of respective fluorescence signals is decreased from $54 \pm 8\%$ in wt AB31 hyphae (measurement of 20 independent filaments) to $46 \pm 18\%$ in $\Delta nma1$ (35 independent hyphae; t -test $p = .0235$). (e) Deletion of *nma1* significantly influences colocalization (left panel) of CORVET subunit Vps3 (mKate2, magenta) and Rab5a (GFP, green). Overlap of respective fluorescence signals is decreased from $43 \pm 13\%$ in wt AB31 hyphae (measurement of 25 independent filaments) to $18 \pm 21\%$ in $\Delta nma1$ (35 independent hyphae; t -test $p < .001$). Kymographs: horizontal scale: 10 s, vertical scale: 10 μm . Significance * p -value $< .05$ ** p -value $< .01$ *** p -value $< .001$. Given are mean values and standard deviation

et al., 2012; Guimaraes et al., 2015; Lin et al., 2016; Marsalek et al., 2017; Olgeiser et al., 2019; Salogiannis et al., 2021) appears to be more critical in *U. maydis* than in *A. nidulans*, where deletion of *hookA* leads to nonmotile EEs and leads to colonies only slightly more compact than those of the wildtype strain (Zhang et al., 2014), while deletion of *hok1* in *U. maydis* leads to severe growth defects (Bielska, Schuster, et al., 2014).

Interestingly, deletion of *vps3* alters the composition of CORVET in *U. maydis*: Vps3 was found to be exchanged with Vps39 (Figure 3d), a subunit of the HOPS complex that interacts with Vps11, a core-subunit present in both HOPS and CORVET (Plemel et al., 2011). For mammalian cells, it has been shown that Vps11 has a similar binding affinity for Vps3 and Vps39 (van der Kant et al., 2015); apparently, the unoccupied binding site of Vps11 for Vps3 in $\Delta vps3$ strains is likely to be adopted by Vps39. In *S. cerevisiae*, such intermediate complexes consisting of Vps8 and Vps39 (i-HOPS) are found during the conversion from CORVET (EEs) to HOPS (late endosomes), and also in *A. nidulans* there is genetic evidence supporting the physiological function of such mixed complexes (Lopez-Berges et al., 2017). As Vps39 interacts with Rab7, the GTPase specific for late endosomes, one could expect that the "i-HOPS" complex is able to interact with both early and late endosomes. Indeed, in $\Delta vps3$ strains, Vps8 and Rab5a were found at increased levels located at static structures (Figures 3e and S7) that could resemble an aggregation of EEs (Rab5) and late endosomes (Rab7), tethered by the Rab7-interaction of Vps39 and the Rab5 interaction of Vps8 of the intermediate "i-HOPS" complex.

As emphasized previously, the contribution to long distance transport is an important expansion in the range of functions for EEs in filamentous fungi. However, despite this "novel" function, the basic components of the endocytic machinery appear to be conserved between yeasts and filamentous fungi. We have now identified the *Nma1* protein with impact on fusion and maturation of EEs, by that modulating the lifespan of EEs as a prerequisite for long distance transport processes.

In $\Delta nma1$ strains, the number of EEs is significantly reduced (Figure 7a). In line with the reduced number, we observe a substantial increase in endosomes with a colocalization of Rab5a and Rab7 (Figure 8a), indicative for an enhanced conversion rate of EEs to late endosomes. The colocalization of Rab5a and Rab7 is known from *A. nidulans* and mammalian cells as an intermediate state

during maturation of EEs (Rab5) to late endosomes (Rab7) (Abenza et al., 2012; Shearer & Petersen, 2019). The increased number of Rab5a/Rab7 endosomes could also lead to extended fusion events mediated by CORVET during transition of EEs to late endosomes, which would explain the fewer, but larger late endosomes observed in $\Delta nma1$ strains (Figure 8b). The prominent Rab5/Rab7 intermediate could also affect the centripetal dynein-mediated transport of mature late endosomes, leading to the observed accumulation of Vps8 (interacting with Rab5a of the Rab5a/Rab7 intermediate endosomes) at the cell poles (Figure S10). For both *A. nidulans* and mammalian cells, it has been described that maturation of EEs to late endosomes is coupled to dynein-mediated transport processes directed inwards from the cell poles to the center (Abenza et al., 2012; Jordens et al., 2001).

How can *Nma1* affect the number of EEs and the conversion rate to late endosomes? We have shown that *Nma1* interacts with the Vps3 protein of CORVET (Figures 3d and 6a,b). Vps3 and Vps8 contact Rab5a-GTPases on membranes of individual endosomes as a first step for membrane fusion. The interaction of *Nma1* with Vps3 could now prevent this "bridging" by the CORVET complex, by that decreasing the fusion rate of microtubule-associated EEs and enhancing the time span of EEs. In addition, *Nma1* could directly affect the conversion rate from EE to late endosomes: one of the initial steps is the recruitment of the GEF for Rab7 by Rab5 to EEs, leading to an increase of GTP-bound Rab7 in the EE membrane and sequentially to the substitution of Rab5 with Rab7 (Langemeyer et al., 2020). It is conceivable that recruitment of the Rab7-GEF by Rab5a is reduced when Rab5a is "occupied" by the *Nma1*-blocked CORVET complex, which would further decrease the conversion rate to late endosomes. The finding that *Nma1* is associated with microtubules would direct the regulatory effect of *Nma1* mostly to the EE population moving on microtubule tracks, that is, exactly the EEs involved in long distance transport for which an extended lifespan would be beneficial. The primary function of *Nma1* is to stabilize the population of EEs as a prerequisite for EE-mediated transport processes.

The interaction of *Nma1* with Vps3 leads also to a stabilization of the binding of Vps3 to the CORVET core complex (Figure 6d,e). In the context that depletion of Vps3 leads to the formation of an intermediate "i-HOPS" complex, the stabilization of the Vps3-CORVET

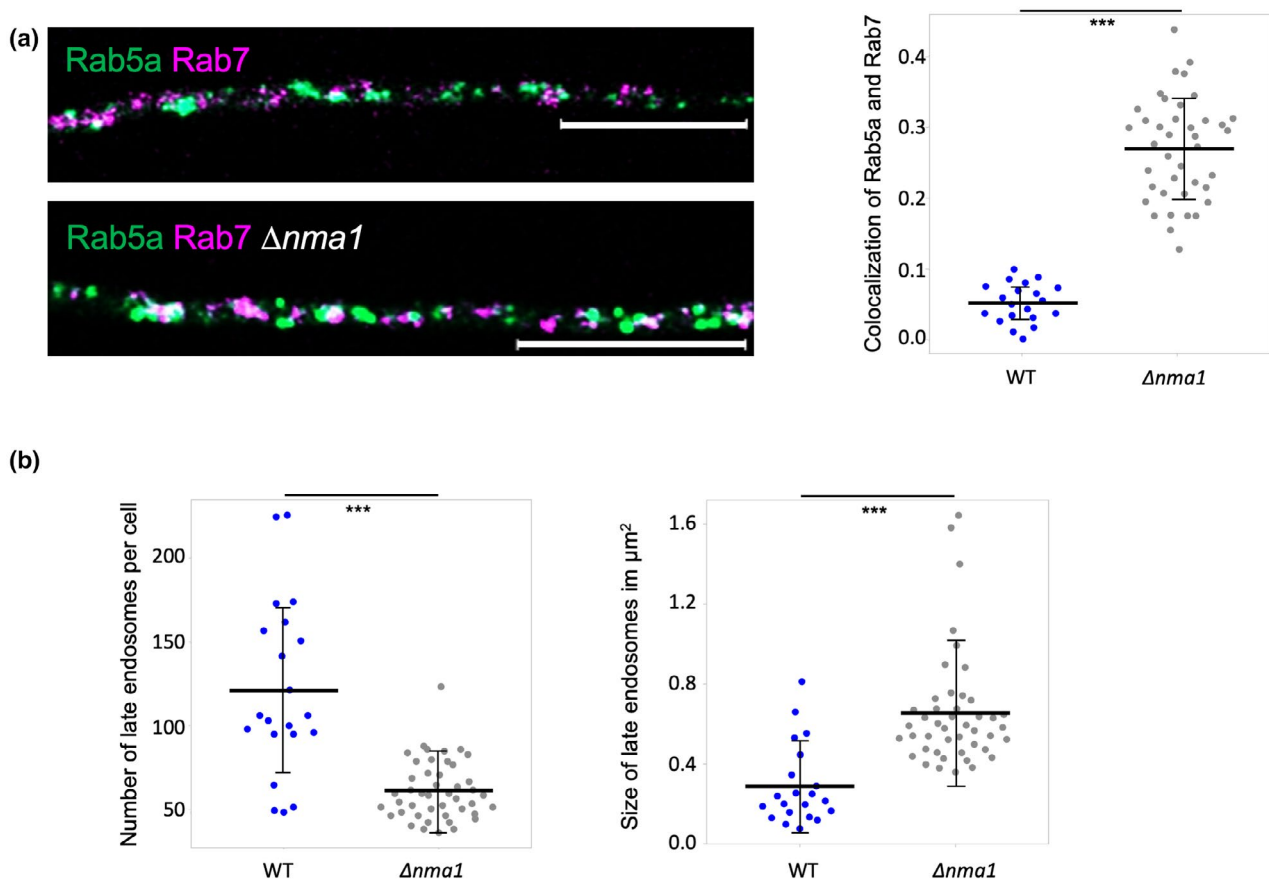


FIGURE 8 Influence of Nma1 on the population of late endosomes. (a) Deletion of *nma1* impacts colocalization (left panel) of endosomal marker proteins Rab5a (GFP, green, early endosomes [EEs]) and Rab7 (mCherry, magenta, late endosomes). Overlap of respective fluorescence signals is enhanced from $5 \pm 3\%$ in wt AB31 hyphae (measurement of 20 independent filaments) to $27 \pm 7\%$ in $\Delta nma1$ (40 independent hyphae; t -test $p < .001$). (b) In AB31 hyphae deletion of *nma1* causes a significant decrease in late endosomes (left panel, wt: 121.7 ± 51 late endosomes ($N = 20$, visualized by mCherry-Rab7) per cell), $\Delta nma1$: 62.8 ± 17.4 ($N = 45$; t -test $p < .001$) in combination with a significant increase in size of late endosome size (right panel, wt: $0.289 \pm 0.2 \mu\text{m}^2$, $\Delta nma1$: $0.65 \pm 0.29 \mu\text{m}^2$, t -test $p < .001$). Horizontal scale: 10 s, vertical scale: 10 μm . Significance * p -value $< .05$ ** p -value $< .01$ *** p -value $< .001$. Given are mean values and standard deviation

interaction may also contribute to a decreased conversion rate of EEs to late endosomes.

In yeasts as *S. cerevisiae*, the function of EEs is mostly restricted to endocytic processes, delivering extracellular cargoes to vacuoles or recycling compartments; in accordance with the spherical cell shape, long distance transport processes play a minor role (reviewed in Mellman, 1996). In filamentous fungi, EEs adopt a prominent role for long distance transport, which, in comparison with yeast EEs, requires a prolonged life span. In *U. maydis*, this process is sustained via Nma1 by modulation endosomal maturation via its influence on the CORVET complex.

4 | EXPERIMENTAL PROCEDURES

4.1 | Strains and growth conditions

Escherichia coli strain TOP10 (Invitrogen, Thermofischer, Carlsbad, CA, USA) was used for cloning. Growth conditions and media for the cultivation of *E. coli* followed the protocols described before (Sambrook et al., 1989). *Saccharomyces cerevisiae* strain AH109 (Clontech/Takara

Bio, Mountain View, CA, USA) was used for yeast two-hybrid interaction studies. *S. cerevisiae* cells were grown in minimal medium (SD) supplemented with the amino acids dropout-mix needed for selection, as described in the Clontech/Takara Bio Matchmaker™ GAL4 Two-Hybrid System 3 Manual (<https://www.takarabio.com>). *U. maydis* cells were grown in YEPSL (Brachmann et al., 2001), CM (complete medium) supplemented with 1% glucose (CM-Glc) or 1% arabinose (CM-Ara), respectively (Holliday, 1974) at 28°C. Solid media contained 2% agar. The induction of hyphal growth in AB31 derivatives was done as previously described in Brachmann et al. (2001). *A. nidulans* was grown in MM (minimal medium) (Hill & Kafer, 2001). All *U. maydis* and *A. nidulans* strains used in this study are listed in Tables S4 and S5, respectively. Growth rate was measured with OD_{600} from three biological replicates and technical duplicates hourly over a time span of 12 hr.

4.2 | Yeast two hybrid test

For interaction studies in yeast, plasmids pGBKT7 and pGADT7 (Clontech/Takara Bio, Mountain View, CA, USA) harboring

U. maydis genes or gene fragments, and the yeast strain AH109 were used, following the protocols given in the Clontech/Takara Bio Matchmaker™ GAL4 Two-Hybrid System 3 Manual (<https://www.takarabio.com>). Plasmids for yeast two hybrid interaction assays are listed in Table S6.

4.3 | DNA procedures

Molecular techniques followed established protocols described in Sambrook et al. (1989). DNA from Agarose gels was extracted following the protocol of Vogelstein and Gillespie (1979). Transformation of *U. maydis* was performed as described earlier (Schulz et al., 1990) with linearized vector DNA or PCR-amplified DNA fragments. Gene deletions and N- and C-terminal gene fusions in *U. maydis* were generated by homologous recombination. Upstream and downstream genomic regions for recombination were obtained by PCR amplification and fused to hygromycin, nourseothricin, or geneticin resistance cassettes for gene deletions or to epitope Tags or open reading frames of fluorescent proteins following published protocols (Brachmann et al., 2004; Kämper, 2004) or by Gibson assembly® (Gibson et al., 2009). Constructs for gene fusions were subcloned in pCR2.1 TOPO (Invitrogen, ThermoFischer Scientific, Carlsbad, CA, USA) and sequenced before transformation. Constructs for genome modification are listed (*U. maydis*: Table S7; *A. nidulans*: Table S8). Sequences of oligonucleotides used for PCR are listed in Table S9. Homologous integration of all constructs was verified by Southern blot analysis (Southern, 1975). Genomic DNA from *U. maydis* was prepared as described in Zhou et al. (2018). DNA from *A. nidulans* was isolated according to Timberlake and Marshall (1989) and transformations were carried out as described in Yelton et al. (1984).

4.4 | Co-immunoprecipitation, western blot, and LC/MS analysis

Co-immunoprecipitation was carried out in vivo with cultures of *U. maydis* AB31 (Brachmann et al., 2001) derivatives, which were grown in 150 ml CM-Glc to an OD₆₀₀ of 0.2 at 28°C on a rotary shaker. Filamentous growth was induced for 7 hr in CM-Ara (Bottin et al., 1996; Brachmann et al., 2001). Cells were washed once with PBS buffer, resuspended in 1 ml PBS, supplemented with “Complete” proteinase inhibitor cocktail (Roche Life Sciences, Penzberg, Germany), frozen in liquid nitrogen, and homogenized in a Retsch Mill MM200 (Retsch, Haan, Germany) for 10 min at 30 Hz. Homogenized cells were centrifuged 2× 30 min; 45,000×g; 4°C (Heraeus Biofuge Stratos, ThermoFischer Scientific, Carlsbad, CA, USA) and the cell pellet was discarded. About 50 µl Pierce™ anti-HA-coupled magnetic beads (ThermoFischer Scientific, Carlsbad, CA, USA) or anti-HA-coupled agarose beads (Sigma-Aldrich, Merck, Taufkirchen, Germany) were washed 3× with 1 ml IP-buffer (25 mM Tris-HCl, 150 mM NaCl, 1 mM EDTA, 5% Glycerin, pH 7.4; modified

after Pierce™), supplemented with “Complete” proteinase inhibitor cocktail (Roche Life Sciences, Penzberg, Germany). About 500 µl cell lysate was incubated with pre-washed beads over night at 4°C on rotating wheel. Beads were washed 5× with 1 ml IP-buffer, supplemented with “Complete” proteinase inhibitor cocktail (Roche Life Sciences, Penzberg, Germany) at 4°C. Magnetic beads were precipitated with DynaMag™-2 magnet rack (Life technologies, ThermoFischer Scientific, Carlsbad, CA, USA), agarose beads were centrifuged (1 min, 5000×g). For elution of precipitated proteins, beads were resuspended 100 µl TE 1% SDS and incubated for 10 min at 65°C and 950 rpm in a rotary heating block. Elution was repeated with 100 µl TE 1% SDS. Combined eluates were filled up for precipitation with 800 µl methanol, 200 µl chloroform, and 600 µl H₂O with vortexing between each step. Samples were centrifuged for 3 min, 16,200×g proteins accumulated in the interphase between the upper and lower phase. The upper phase was removed, and proteins were precipitated by addition of 600 µl methanol, vortexing and centrifugation (16,200×g, 10 min). Protein pellets were dissolved in 40 µl 1xRoti®Load (Carl Roth, Karlsruhe, Germany). Proteins were separated by SDS-polyacrylamide-gel electrophoresis (PAGE) (Laemmli, 1970) in Mini Protean II cells (BioRad, Hercules, CA, USA) on 10% acrylamide gels (30 min 20 mA⁻¹; 60 min 30 mA⁻¹). PAGERuler Prestained Protein Marker (ThermoFischer Scientific, Carlsbad, CA, USA) or Color Prestained Protein Standard, Broad Range (NEB, Ipswich, MA, USA) was used as standards. Separated proteins were transferred to PVDF nitrocellulose membranes (Roti®-PVDF; Carl Roth, Karlsruhe, Germany) with discontinuous, semi-dry blotting unit (Fastblot B43 Biometra, Göttingen, Germany; 18 min 2 mA⁻¹ per cm² membrane) (Towbin et al., 1979). Proteins were detected using the ECL system, following the protocol provided by the manufacturer (ThermoFischer Scientific, Carlsbad, CA, USA) with LI-COR ODYSSEY FC Mod. 2800 (Li-Cor, Lincoln, NE, USA). Monoclonal anti-HA or anti-c-Myc (Sigma-Aldrich, Merck, Taufkirchen, Germany) antibodies were used as primary probes, and Horseradish peroxidase-conjugated anti-rabbit IgG (Promega, Madison, WI, USA) was used as secondary antibody.

For LC/MS analysis, protein samples were trypsin-digested with an in-gel digestion following the protocol in Shevchenko et al. (1996). Samples were purified using the C18 stage tipping method (Rappsilber et al., 2003, 2007). The peptide solution was vacuum dried and dissolved in sample buffer (2% acetonitrile, 0.1% formic acid) for LC/MS analysis (Nanoflow liquid chromatography RSLCnano Ultimate 3000 system coupled to nano electrospray mass spectrometer); 4 µl peptide solution with 0.07% trifluoro acetic acid were loaded on Acclaim® PepMAP RSLC columns (75 µm × 50 cm (#164,540), C18, 3 µm, 100 Å) with 20 µl/min flow rate with 3 min duration; followed by a reversed phase chromatography via Acclaim® PepMAP RSLC column (75 µm × 50 cm (#164,540), C18, 3 µm, 100 Å) with a gradient of 96% solvent A (0.1% formic acid) and 4% solvent B (80% acetonitrile, 0.1% formic acid) to 45% solvent B for 82 min; following 90% solvent B/12 min and contrast flow of 90% solvent B/3 min; flow rate of gradient 300 nl/min. Ionization of peptides was carried out on-line with nano electrospray at 1.5 kV (Nanospray Flex™ ion

source) and transferred in mass spectrometer (Q Exactive HF). Full scans were performed in the range of 300–1800 *m/z* (Orbitrap-FT Analyzer, resolution 60.000 and data-dependent top 10 MS2 fragmentation (HCD; resolution 15.000)). All equipments used for LC/MS analysis were from ThermoFischer Scientific, Carlsbad, CA, USA. For programming and collection of data, XCalibur 4.0 software (ThermoFischer Scientific, Carlsbad, CA, USA) was used. LC/MS was performed by the Service Unit LCMS Protein Analysis, Georg-August University Göttingen. MS-data were analyzed with MaxQuant 1.6.0.16 (Tyanova et al., 2016) (<https://maxquant.org>).

4.5 | Microscopy, image processing, and quantitative analysis

For microscopic analyses, logarithmically growing *U. maydis* AB31 (Brachmann et al., 2001) derivatives were grown in 10 ml CM-Glc to an OD₆₀₀ of 0.5 at 28°C on a rotary shaker. For the induction of hyphal growth, cells were shifted to CM-Ara for 15–18 hr.

For microscopy of *A. nidulans* germlings and young hyphae, MM on cover slips was inoculated with a small amount of spores and incubated for 12–18 hr at 37°C.

By Axioimager Z1 microscope (Carl Zeiss, Jena, Germany), cells were then placed on top of a 2% agarose cushion placed on the microscope slide and immediately observed. Standard filter sets for DAPI (353/465 nm), GFP (488/509 nm), and RFP (mCherry/mKate2; 545–590 nm/572–612 nm) were used for epifluorescence analysis. For the visualization of vacuoles, growing cells were incubated in CM supplemented with 10 mg/ml CellTracker Blue (7-amino-4-chloromethyl-ethyl-coumarin, CMAC) (Invitrogen, ThermoFischer, Carlsbad, CA, USA) for 30 min at RT, washed twice with CM, and then subjected to microscopy.

For microscopy with the LSM 800/LSM 900 invers microscopes (Carl Zeiss, Jena, Germany), cells were mixed 1:1 with 4% low gelling agarose (Sigma Agarose Typ VII: Low Gelling Temperature) and transferred to a microscopy chamber (μ -Slide 8 Well Glass Bottom, ibidi GmbH, Gräfelfing, Germany). Endosome motility was recorded in image sequences with 1 min duration, taken with an exposure time of 100 ms. The resulting movies were “bleach corrected” (histogram matching) and converted into kymographs (Plugin kymograph builder) using Fiji ImageJ software (Schindelin et al., 2012, 2015; Schneider et al., 2012). The scale of kymographs was calculated with “set scale:” (distance: 9.7674 distance in pixels, known distance 1.00, pixel aspect ratio 1.0, unit micron; time: 10 distance in pixels, known distance 1.00, pixel aspect ratio 1.0, unit s). Quantification of vesicles (number and average size) was performed with 8-bit converted microscopic images of 100 ms exposure time in Fiji ImageJ software (Schindelin et al., 2012, 2015; Schneider et al., 2012). Reduction of background signal with “median filter” (process—filters—median, 1 pixel radius) and subtraction of background (process—subtract background, with values rolling = 5 pixels, sliding paraboloid). To sharpen borders of objects laces were reinforced (image—adjust—auto local threshold with parameters Bernsen, radius = 15,

parameter 1 = 0, parameter 2 = 0, white objects on black background). Measurement of vesicles was performed (analyze—analyze particles with parameters size 0-Infinity, circularity 0.00–1.00, display results, summarize). Analysis of fluorescence signal colocalization was performed with 8-bit converted microscopic images of 100 ms exposure time in Fiji ImageJ software (Schindelin et al., 2012, 2015; Schneider et al., 2012).

Images for quantification of colocalization were processed prior to measurement as follows: Reduction of background signal with “median filter,” subtraction of background, and reinforcement of object borders were performed as described above for vesicle quantification. Measurement of signal overlaps with JACoP plugin (Manders1&Manders2 coefficient). The M1&M2 coefficient is summing the intensities of pixels from one channel and dividing the sum by its integrated density. A pixel from the GFP channel is considered as colocalized if it has a nonzero intensity counterpart in the mCherry channel. The M1&M2 coefficients give an estimate of the amount of colocalizing signal from a signal over another, without making any assumption on the stoichiometry it may adopt (Bolte & Cordelieres, 2006).

All image processing, including adjustment of brightness, contrast, and gamma-values was performed with the AxioVision and ZEN software (Carl Zeiss, Jena, Germany), respectively.

4.6 | Visualization of data

For visualization of data, the web source PlotsOfData was used <https://huygens.science.uva.nl/PlotsOfData/> (Postma & Goedhart, 2019).

ACKNOWLEDGMENTS

Ka.S. and J.K. like to thank Matteo Jurca for providing plasmid pMF5-9g, Lukas Baumann for help with Y2H experiments, Rabea Suhrborg for constructions of the *U. maydis* strains URS3 and URS6, and Kai Heibel for his helpful comments and suggestions for the manuscript. Open Access funding enabled and organized by Projekt DEAL.

AUTHOR CONTRIBUTIONS

Karina Schneider, Theresa Farr, and Jörg Kämper designed the project; Karina Schneider and Theresa Farr conducted experiments, MS-experiments were performed by Kerstin Schmitt, Oliver Valerius, and Gerhard H. Braus. Data were analyzed by Karina Schneider, Theresa Farr, Niko Pinter, Kerstin Schmitt, and Oliver Valerius; Karina Schneider and Jörg Kämper wrote the manuscript.

DATA AVAILABILITY STATEMENT

The data that supports the findings of this study are available in the supplementary material of this article. Additional, data and material are available from the corresponding author upon reasonable request.

ORCID

Gerhard H. Braus  <https://orcid.org/0000-0002-3117-5626>

Jörg Kämper  <https://orcid.org/0000-0002-8161-5431>

REFERENCES

- Abenza, J.F., Galindo, A., Pantazopoulou, A., Gil, C. de los Rios, V., & Penalva, M.A. (2010) *Aspergillus* RabB Rab5 integrates acquisition of degradative identity with the long distance movement of early endosomes. *Molecular Biology of the Cell*, *21*, 2756–2769.
- Abenza, J.F., Galindo, A., Pinar, M., Pantazopoulou, A., de los Rios, V., & Penalva, M.A. (2012) Endosomal maturation by Rab conversion in *Aspergillus nidulans* is coupled to dynein-mediated basipetal movement. *Molecular Biology of the Cell*, *23*, 1889–1901.
- Abenza, J.F., Pantazopoulou, A., Rodriguez, J.M., Galindo, A. & Penalva, M.A. (2009) Long-distance movement of *Aspergillus nidulans* early endosomes on microtubule tracks. *Traffic*, *10*, 57–75. <https://doi.org/10.1111/j.1600-0854.2008.00848.x>
- Balderhaar, H.J., Lachmann, J., Yavavli, E., Brocker, C., Lurick, A. & Ungermann, C. (2013) The CORVET complex promotes tethering and fusion of Rab5/Vps21-positive membranes. *Proceedings of the National Academy of Sciences USA*, *110*, 3823–3828. <https://doi.org/10.1073/pnas.1221785110>
- Balderhaar, H.J. & Ungermann, C. (2013) CORVET and HOPS tethering complexes—coordinators of endosome and lysosome fusion. *Journal of Cell Science*, *126*, 1307–1316.
- Banuett, F. & Herskowitz, I. (1989) Different *a* alleles of *Ustilago maydis* are necessary for maintenance of filamentous growth but not for meiosis. *Proceedings of the National Academy of Sciences of the USA*, *86*, 5878–5882. <https://doi.org/10.1073/pnas.86.15.5878>
- Baumann, S., Pohlmann, T., Jungbluth, M., Brachmann, A. & Feldbrügge, M. (2012) Kinesin-3 and dynein mediate microtubule-dependent co-transport of mRNPs and endosomes. *Journal of Cell Science*, *125*, 2740–2752. <https://doi.org/10.1242/jcs.101212>
- Becht, P., König, J. & Feldbrügge, M. (2006) The RNA-binding protein Rrm4 is essential for polarity in *Ustilago maydis* and shuttles along microtubules. *Journal of Cell Science*, *119*, 4964–4973.
- Bielska, E., Higuchi, Y., Schuster, M., Steinberg, N., Kilaru, S., Talbot, N.J. et al. (2014) Long-distance endosome trafficking drives fungal effector production during plant infection. *Nature Communications*, *5*, 5097. <https://doi.org/10.1038/ncomms6097>
- Bielska, E., Schuster, M., Roger, Y., Berepiki, A., Soanes, D.M., Talbot, N.J. et al. (2014) Hook is an adapter that coordinates kinesin-3 and dynein cargo attachment on early endosomes. *Journal of Cell Biology*, *204*, 989–1007. <https://doi.org/10.1083/jcb.201309022>
- Bolte, S. & Cordelieres, F.P. (2006) A guided tour into subcellular colocalization analysis in light microscopy. *Journal of Microscopy*, *224*, 213–232. <https://doi.org/10.1111/j.1365-2818.2006.01706.x>
- Bottin, A., Kämper, J. & Kahmann, R. (1996) Isolation of a carbon source-regulated gene from *Ustilago maydis*. *Molecular and General Genetics*, *253*, 342–352.
- Brachmann, A., König, J., Julius, C. & Feldbrügge, M. (2004) A reverse genetic approach for generating gene replacement mutants in *Ustilago maydis*. *Molecular Genetics and Genomics: MGG*, *272*, 216–226. <https://doi.org/10.1007/s00438-004-1047-z>
- Brachmann, A., Weinzierl, G., Kämper, J. & Kahmann, R. (2001) Identification of genes in the bW/bE regulatory cascade in *Ustilago maydis*. *Molecular Microbiology*, *42*, 1047–1063.
- Brefort, T., Doehlemann, G., Mendoza-Mendoza, A., Reissmann, S., Djamei, A. & Kahmann, R. (2009) *Ustilago maydis* as a pathogen. *Annual Review of Phytopathology*, *47*, 423–445.
- Bröcker, C., Kuhlee, A., Gatsogiannis, C., Balderhaar, H.J., Hönscher, C., Engelbrecht-Vandre, S. et al. (2012) Molecular architecture of the multisubunit homotypic fusion and vacuole protein sorting (HOPS) tethering complex. *Proceedings of the National Academy of Sciences USA*, *109*, 1991–1996. <https://doi.org/10.1073/pnas.1117797109>
- Casanova, J.E. & Winckler, B. (2017) A new Rab7 effector controls phosphoinositide conversion in endosome maturation. *Journal of Cell Biology*, *216*, 2995–2997. <https://doi.org/10.1083/jcb.201709034>
- Christensen, J.R., Kendrick, A.A., Truong, J.B., Aguilar-Maldonado, A., Adani, V., Dzieciatkowska, M. et al. (2021) Cytoplasmic dynein-1 cargo diversity is mediated by the combinatorial assembly of FTS-Hook-FHIP complexes. *bioRxiv*. <https://doi.org/10.1101/2021.10.07.463551>
- Christoforidis, S., McBride, H.M., Burgoyne, R.D. & Zerial, M. (1999) The Rab5 effector EEA1 is a core component of endosome docking. *Nature*, *397*, 621–625. <https://doi.org/10.1038/17618>
- Diaz, R., Mayorga, L. & Stahl, P. (1988) In vitro fusion of endosomes following receptor-mediated endocytosis. *Journal of Biological Chemistry*, *263*, 6093–6100. [https://doi.org/10.1016/S0021-9258\(18\)68754-X](https://doi.org/10.1016/S0021-9258(18)68754-X)
- Freitag, J., Lanver, D., Böhmer, C., Schink, K.O., Bölker, M. & Sandrock, B. (2011) Septation of infectious hyphae is critical for appressoria formation and virulence in the smut fungus *Ustilago maydis*. *PLoS Path.*, *7*, e1002044. <https://doi.org/10.1371/journal.ppat.1002044>
- Fuchs, U., Hause, G., Schuchardt, I. & Steinberg, G. (2006) Endocytosis is essential for pathogenic development in the corn smut fungus *Ustilago maydis*. *The Plant Cell*, *18*, 2066–2081.
- Gallwitz, D., Donath, C. & Sander, C. (1983) A yeast gene encoding a protein homologous to the human c-has/bas proto-oncogene product. *Nature*, *306*, 704–707. <https://doi.org/10.1038/306704a0>
- Gibson, D.G., Young, L., Chuang, R.Y., Venter, J.C., Hutchison, C.A. 3rd & Smith, H.O. (2009) Enzymatic assembly of DNA molecules up to several hundred kilobases. *Nature Methods*, *6*, 343–345. <https://doi.org/10.1038/nmeth.1318>
- Göhre, V., Vollmeister, E., Bölker, M. & Feldbrügge, M. (2012) Microtubule-dependent membrane dynamics in *Ustilago maydis*: trafficking and function of Rab5a-positive endosomes. *Communicative & Integrative Biology*, *5*, 485–490.
- Guimaraes, S.C., Schuster, M., Bielska, E., Dagdas, G., Kilaru, S., Meadoes, B.R. et al. (2015) Peroxisomes, lipid droplets, and endoplasmic reticulum “hitchhike” on motile early endosomes. *Journal of Cell Biology*, *211*, 945–954. <https://doi.org/10.1083/jcb.201505086>
- Guo, X., Farias, G.G., Mattera, R. & Bonifacino, J.S. (2016) Rab5 and its effector FHF contribute to neuronal polarity through dynein-dependent retrieval of somatodendritic proteins from the axon. *Proceedings of the National Academy of Sciences USA*, *113*, E5318–E5327. <https://doi.org/10.1073/pnas.1601844113>
- Higuchi, Y., Ashwin, P., Roger, Y. & Steinberg, G. (2014) Early endosome motility spatially organizes polysome distribution. *Journal of Cell Biology*, *204*, 343–357. <https://doi.org/10.1083/jcb.201307164>
- Hill, T.W. & Kafer, E. (2001) Improved protocols for *Aspergillus* minimal medium: trace element and minimal medium salt stock solutions. *Fungal Genetics Reports*, *48*, 20–21. <https://doi.org/10.4148/1941-4765.1173>
- Holliday, R. (1974) *Ustilago maydis*. In: King, R.C. (Ed.) *Handbook of genetics*. Plenum Press, pp. 575–595.
- Homma, Y., Hiragi, S. & Fukuda, M. (2021) Rab family of small GTPases: an updated view on their regulation and functions. *FEBS Journal*, *288*, 36–55. <https://doi.org/10.1111/febs.15453>
- Huang, C.E., Milutinovich, M. & Koshland, D. (2005) Rings, bracelet or snaps: fashionable alternatives for Smc complexes. *Philosophical Transactions of the Royal Society of London. Series B, Biological Sciences*, *360*, 537–542. <https://doi.org/10.1098/rstb.2004.1609>
- Jordens, I., Fernandez-Borja, M., Marsman, M., Dusseljee, S., Janssen, L., Calafat, J. et al. (2001) The Rab7 effector protein RILP controls lysosomal transport by inducing the recruitment of dynein-dynactin motors. *Current Biology*, *11*, 1680–1685. [https://doi.org/10.1016/S0960-9822\(01\)00531-0](https://doi.org/10.1016/S0960-9822(01)00531-0)
- Kämper, J. (2004) A PCR-based system for highly efficient generation of gene replacement mutants in *Ustilago maydis*. *Molecular Genetics and Genomics: MGG*, *271*, 103–110. <https://doi.org/10.1007/s00438-003-0962-8>
- Klöpffer, T.H., Kienle, N., Fasshauer, D. & Munro, S. (2012) Untangling the evolution of Rab G proteins: implications of a comprehensive genomic analysis. *BMC Biology*, *10*, 71. <https://doi.org/10.1186/1741-7007-10-71>

- Laemmli, U.K. (1970) Cleavage of structural proteins during the assembly of the head of bacteriophage T4. *Nature*, **227**, 680–685.
- Langemeyer, L., Borchers, A.C., Herrmann, E., Fullbrunn, N., Han, Y., Perz, A. et al. (2020) A conserved and regulated mechanism drives endosomal Rab transition. *eLife*, **9**, e56090. <https://doi.org/10.7554/eLife.56090>
- Langemeyer, L., Frohlich, F. & Ungermann, C. (2018) Rab GTPase function in endosome and lysosome biogenesis. *Trends in Cell Biology*, **28**, 957–970. <https://doi.org/10.1016/j.tcb.2018.06.007>
- Lazar, T., Gotte, M. & Gallwitz, D. (1997) Vesicular transport: how many Ypt/Rab-GTPases make a eukaryotic cell? *Trends in Biochemical Sciences*, **22**, 468–472. [https://doi.org/10.1016/S0968-0004\(97\)01150-X](https://doi.org/10.1016/S0968-0004(97)01150-X)
- Liang, C., Lee, J.S., Inn, K.S., Gack, M.U., Li, Q., Roberts, E.A. et al. (2008) Beclin1-binding UVRAG targets the class C Vps complex to coordinate autophagosome maturation and endocytic trafficking. *Nature Cell Biology*, **10**, 776–787. <https://doi.org/10.1038/ncb1740>
- Lin, C., Schuster, M., Guimaraes, S.C., Ashwin, P., Schrader, M., Metz, J. et al. (2016) Active diffusion and microtubule-based transport oppose myosin forces to position organelles in cells. *Nature Communications*, **7**, 11814. <https://doi.org/10.1038/ncomms11814>
- Lopez-Berges, M.S., Arst, H.N., Pinar, M. & Penalva, M.A. (2017) Genetic studies on the physiological role of CORVET in *Aspergillus nidulans*. *FEMS Microbiology Letters*, **364**, fnx065. <https://doi.org/10.1093/femsle/fnx065>
- Lörincz, P., Lakatos, Z., Varga, A., Maruzs, T., Simon-Vecsei, Z., Darula, Z. et al. (2016) MiniCORVET is a Vps8-containing early endosomal tether in *Drosophila*. *eLife*, **5**, e14226. <https://doi.org/10.7554/eLife.14226>
- Losada, A. & Hirano, T. (2005) Dynamic molecular linkers of the genome: the first decade of SMC proteins. *Genes & Development*, **19**, 1269–1287. <https://doi.org/10.1101/gad.1320505>
- Marsalek, L., Gruber, C., Altmann, F., Aleschko, M., Mattanovich, D., Gasser, B. et al. (2017) Disruption of genes involved in CORVET complex leads to enhanced secretion of heterologous carboxylesterase only in protease deficient *Pichia pastoris*. *Biotechnology Journal*, **12**, 1600584. <https://doi.org/10.1002/biot.201600584>
- Mellman, I. (1996) Endocytosis and molecular sorting. *Annual Review of Cell and Developmental Biology*, **12**, 575–625. <https://doi.org/10.1146/annurev.cellbio.12.1.575>
- Nasmyth, K. & Haering, C.H. (2005) The structure and function of SMC and kleisin complexes. *Annual Review of Biochemistry*, **74**, 595–648. <https://doi.org/10.1146/annurev.biochem.74.082803.133219>
- Olgeiser, L., Haag, C., Boerner, S., Ule, J., Busch, A., Koepke, J., et al. (2019) The key protein of endosomal mRNP transport Rrm4 binds translational landmark sites of cargo mRNAs. *EMBO Reports*, **20**, e46588. <https://doi.org/10.15252/embr.201846588>
- Ostrowicz, C.W., Bocker, C., Ahnert, F., Nordmann, M., Lachmann, J., Peplowska, K. et al. (2010) Defined subunit arrangement and rab interactions are required for functionality of the HOPS tethering complex. *Traffic*, **11**, 1334–1346. <https://doi.org/10.1111/j.1600-0854.2010.01097.x>
- Pawelec, A., Arsic, J. & Kolling, R. (2010) Mapping of Vps21 and HOPS binding sites in Vps8 and effect of binding site mutants on endocytic trafficking. *Eukaryotic Cell*, **9**, 602–610. <https://doi.org/10.1128/EC.00286-09>
- Peplowska, K., Markgraf, D.F., Ostrowicz, C.W., Bange, G. & Ungermann, C. (2007) The CORVET tethering complex interacts with the yeast Rab5 homolog Vps21 and is involved in endo-lysosomal biogenesis. *Developmental Cell*, **12**, 739–750. <https://doi.org/10.1016/j.devcel.2007.03.006>
- Pereira-Leal, J.B. (2008) The Ypt/Rab family and the evolution of trafficking in fungi. *Traffic*, **9**, 27–38. <https://doi.org/10.1111/j.1600-0854.2007.00667.x>
- Perini, E.D., Schaefer, R., Stoter, M., Kalaidzidis, Y. & Zerial, M. (2014) Mammalian CORVET is required for fusion and conversion of distinct early endosome subpopulations. *Traffic*, **15**, 1366–1389. <https://doi.org/10.1111/tra.12232>
- Pinar, M. & Penalva, M.A. (2021) The fungal RABOME: Rab GTPases acting in the endocytic and exocytic pathways of *Aspergillus nidulans* (with excursions to other filamentous fungi). *Molecular Microbiology*, **116**, 53–70.
- Plemel, R.L., Lobingier, B.T., Brett, C.L., Angers, C.G., Nickerson, D.P., Paulsel, A. et al. (2011) Subunit organization and Rab interactions of Vps-C protein complexes that control endolysosomal membrane traffic. *Molecular Biology of the Cell*, **22**, 1353–1363. <https://doi.org/10.1091/mbc.e10-03-0260>
- Postma, M. & Goedhart, J. (2019) PlotsOfData-A web app for visualizing data together with their summaries. *PLoS Biology*, **17**, e3000202. <https://doi.org/10.1371/journal.pbio.3000202>
- Poteryaev, D., Datta, S., Ackema, K., Zerial, M. & Spang, A. (2010) Identification of the switch in early-to-late endosome transition. *Cell*, **141**, 497–508. <https://doi.org/10.1016/j.cell.2010.03.011>
- Rappsilber, J., Ishihama, Y. & Mann, M. (2003) Stop and go extraction tips for matrix-assisted laser desorption/ionization, nano-electrospray, and LC/MS sample pretreatment in proteomics. *Analytical Chemistry*, **75**, 663–670. <https://doi.org/10.1021/ac026117i>
- Rappsilber, J., Mann, M. & Ishihama, Y. (2007) Protocol for micro-purification, enrichment, pre-fractionation and storage of peptides for proteomics using StageTips. *Nature Protocols*, **2**, 1896–1906. <https://doi.org/10.1038/nprot.2007.261>
- Rink, J., Ghigo, E., Kalaidzidis, Y. & Zerial, M. (2005) Rab conversion as a mechanism of progression from early to late endosomes. *Cell*, **122**, 735–749. <https://doi.org/10.1016/j.cell.2005.06.043>
- Salogiannis, J., Christensen, J.R., Songster, L.D., Aguilar-Maldonado, A., Shukla, N. & Reck-Peterson, S.L. (2021) PxdA interacts with the DipA phosphatase to regulate peroxisome hitchhiking on early endosomes. *Molecular Biology of the Cell*, **32**, 492–503. <https://doi.org/10.1091/mbc.E20-08-0559>
- Sambrook, J., Fritsch, E.F. & Maniatis, T. (1989) *Molecular cloning: a laboratory manual*. Cold Spring Harbour Laboratory Press.
- Schindelin, J., Arganda-Carreras, I., Frise, E., Kaynig, V., Longair, M., Pietzsch, T. et al. (2012) Fiji: an open-source platform for biological-image analysis. *Nature Methods*, **9**, 676–682. <https://doi.org/10.1038/nmeth.2019>
- Schindelin, J., Rueden, C.T., Hiner, M.C. & Eliceiri, K.W. (2015) The ImageJ ecosystem: an open platform for biomedical image analysis. *Molecular Reproduction and Development*, **82**, 518–529. <https://doi.org/10.1002/mrd.22489>
- Schneider, C.A., Rasband, W.S. & Eliceiri, K.W. (2012) NIH image to ImageJ: 25 years of image analysis. *Nature Methods*, **9**, 671–675. <https://doi.org/10.1038/nmeth.2089>
- Schulz, B., Banuett, F., Dahl, M., Schlesinger, R., Schäfer, W., Martin, T. et al. (1990) The *b* alleles of *U. maydis*, whose combinations program pathogenic development, code for polypeptides containing a homeodomain-related motif. *Cell*, **60**, 295–306. [https://doi.org/10.1016/0092-8674\(90\)90744-Y](https://doi.org/10.1016/0092-8674(90)90744-Y)
- Schuster, M., Kilaru, S., Ashwin, P., Lin, C., Severs, N.J. & Steinberg, G. (2011) Controlled and stochastic retention concentrates dynein at microtubule ends to keep endosomes on track. *The EMBO Journal*, **30**, 652–664.
- Schuster, M., Kilaru, S., Fink, G., Collemare, J., Roger, Y. & Steinberg, G. (2011) Kinesin-3 and dynein cooperate in long-range retrograde endosome motility along a nonuniform microtubule array. *Molecular Biology of the Cell*, **22**, 3645–3657.
- Scott, C.C., Vacca, F. & Gruenberg, J. (2014) Endosome maturation, transport and functions. *Seminars in Cell & Developmental Biology*, **31**, 2–10. <https://doi.org/10.1016/j.semcdb.2014.03.034>
- Shearer, L.J. & Petersen, N.O. (2019) Distribution and co-localization of endosome markers in cells. *Heliyon*, **5**, e02375. <https://doi.org/10.1016/j.heliyon.2019.e02375>

- Shevchenko, A., Wilm, M., Vorm, O. & Mann, M. (1996) Mass spectrometric sequencing of proteins silver-stained polyacrylamide gels. *Analytical Chemistry*, *68*, 850–858.
- Singer-Krüger, B., Stenmark, H., Düsterhöft, A., Philippsen, P., Yoo, J.S., Gallwitz, D. et al. (1994) Role of three rab5-like GTPases, Ypt51p, Ypt52p, and Ypt53p, in the endocytic and vacuolar protein sorting pathways of yeast. *Journal of Cell Biology*, *125*, 283–298. <https://doi.org/10.1083/jcb.125.2.283>
- Solinger, J.A. & Spang, A. (2013) Tethering complexes in the endocytic pathway: CORVET and HOPS. *FEBS Journal*, *280*, 2743–2757. <https://doi.org/10.1111/febs.12151>
- Southern, E.M. (1975) Detection of specific sequences among DNA fragments separated by gel electrophoresis. *Journal of Molecular Biology*, *98*, 503–517. [https://doi.org/10.1016/S0022-2836\(75\)80083-0](https://doi.org/10.1016/S0022-2836(75)80083-0)
- Steinberg, G. & Perez-Martin, J. (2008) *Ustilago maydis*, a new fungal model system for cell biology. *Trends in Cell Biology*, *18*, 61–67. <https://doi.org/10.1016/j.tcb.2007.11.008>
- Stroupe, C., Collins, K.M., Fratti, R.A. & Wickner, W. (2006) Purification of active HOPS complex reveals its affinities for phosphoinositides and the SNARE Vam7p. *EMBO Journal*, *25*, 1579–1589. <https://doi.org/10.1038/sj.emboj.7601051>
- Timberlake, W.E. & Marshall, M.A. (1989) Genetic engineering of filamentous fungi. *Science*, *244*, 1313–1317. <https://doi.org/10.1126/science.2525275>
- Torng, T., Song, H. & Wickner, W. (2020) Asymmetric Rab activation of vacuolar HOPS to catalyze SNARE complex assembly. *Molecular Biology of the Cell*, *31*, 1060–1068. <https://doi.org/10.1091/mbc.E20-01-0019>
- Towbin, H., Staehelin, T. & Gordon, J. (1979) Electrophoretic transfer of proteins from polyacrylamide gels to nitrocellulose sheets—procedure and some applications. *Proceedings of the National Academy of Sciences USA*, *76*, 4350–4354. <https://doi.org/10.1073/pnas.76.9.4350>
- Tyanova, S., Temu, T. & Cox, J. (2016) The MaxQuant computational platform for mass spectrometry-based shotgun proteomics. *Nature Protocols*, *11*, 2301–2319. <https://doi.org/10.1038/nprot.2016.136>
- Ungermann, C. & Kümmel, D. (2019) Structure of membrane tethers and their role in fusion. *Traffic*, *20*, 479–490. <https://doi.org/10.1111/tra.12655>
- van der Kant, R., Jonker, C.T., Wijdeven, R.H., Bakker, J., Janssen, L., Klumperman, J. et al. (2015) Characterization of the mammalian CORVET and HOPS complexes and their modular restructuring for endosome specificity. *Journal of Biological Chemistry*, *290*, 30280–30290. <https://doi.org/10.1074/jbc.M115.688440>
- Vogelstein, B. & Gillespie, D. (1979) Preparative and analytical purification of DNA from agarose. *Proceedings of the National Academy of Sciences USA*, *76*, 615–619. <https://doi.org/10.1073/pnas.76.2.615>
- Wedlich-Söldner, R., Bölker, M., Kahmann, R. & Steinberg, G. (2000) A putative endosomal t-SNARE links exo- and endocytosis in the phytopathogenic fungus *Ustilago maydis*. *EMBO Journal*, *19*, 1974–1986. <https://doi.org/10.1093/emboj/19.9.1974>
- Xu, L., Sowa, M.E., Chen, J., Li, X., Gygi, S.P. & Harper, J.W. (2008) An FTS/Hook/p107(FHIP) complex interacts with and promotes endosomal clustering by the homotypic vacuolar protein sorting complex. *Molecular Biology of the Cell*, *19*, 5059–5071.
- Yao, X., Wang, X. & Xiang, X. (2014) FHIP and FTS proteins are critical for dynein-mediated transport of early endosomes in *Aspergillus*. *Molecular Biology of the Cell*, *25*, 2181–2189.
- Yelton, M.M., Hamer, J.E. & Timberlake, W.E. (1984) Transformation of *Aspergillus nidulans* by using a trpC plasmid. *Proceedings of the National Academy of Sciences USA*, *81*, 1470–1474. <https://doi.org/10.1073/pnas.81.5.1470>
- Yogosawa, S., Hatakeyama, S., Nakayama, K.I., Miyoshi, H., Kohsaka, S. & Akazawa, C. (2005) Ubiquitylation and degradation of serum-inducible kinase by hVPS18, a RING-H2 type ubiquitin ligase. *Journal of Biological Chemistry*, *280*, 41619–41627. <https://doi.org/10.1074/jbc.M508397200>
- Yogosawa, S., Kawasaki, M., Wakatsuki, S., Kominami, E., Shiba, Y., Nakayama, K. et al. (2006) Monoubiquitylation of GGA3 by hVPS18 regulates its ubiquitin-binding ability. *Biochemical and Biophysical Research Communications*, *350*, 82–90. <https://doi.org/10.1016/j.bbrc.2006.09.013>
- Zander, S., Baumann, S., Weidtkamp-Peters, S. & Feldbrügge, M. (2016) Endosomal assembly and transport of heteromeric septin complexes promote septin cytoskeleton formation. *Journal of Cell Science*, *129*, 2778–2792. <https://doi.org/10.1242/jcs.182824>
- Zerial, M. & McBride, H. (2001) Rab proteins as membrane organizers. *Nature Reviews Molecular Cell Biology*, *2*, 107–117. <https://doi.org/10.1038/35052055>
- Zhang, J., Qiu, R., Arst, H.N. Jr, Penalva, M.A. & Xiang, X. (2014) HookA is a novel dynein-early endosome linker critical for cargo movement in vivo. *Journal of Cell Biology*, *204*, 1009–1026. <https://doi.org/10.1083/jcb.201308009>
- Zhou, L., Obhof, T., Schneider, K., Feldbrügge, M., Nienhaus, G.U. & Kämper, J. (2018) Cytoplasmic transport machinery of the SPF27 homologue Num1 in *Ustilago maydis*. *Scientific Reports*, *8*, 3611. <https://doi.org/10.1038/s41598-018-21628-y>
- Zick, M. & Wickner, W. (2016) Improved reconstitution of yeast vacuole fusion with physiological SNARE concentrations reveals an asymmetric Rab(GTP) requirement. *Molecular Biology of the Cell*, *27*, 2590–2597. <https://doi.org/10.1091/mbc.e16-04-0230>

SUPPORTING INFORMATION

Additional supporting information may be found in the online version of the article at the publisher's website.

How to cite this article: Schneider, K., Farr, T., Pinter, N., Schmitt, K., Valerius, O., Braus, G.H., et al (2021) The Nma1 protein promotes long distance transport mediated by early endosomes in *Ustilago maydis*. *Molecular Microbiology*, *00*, 1–19. <https://doi.org/10.1111/mmi.14851>